Ahn *et al. Earth, Planets and Space* (2018) 70:78
https://doi.org/10.1186/s40623-018-0850-4

Earth, Planets and Space

FULL PAPER

Open Access

Preliminary paleomagnetic and rock magnetic results from 17 to 22 ka sediment of Jeju Island, Korea: Geomagnetic excursional behavior or rock magnetic anomalies?

Hyeon-Seon Ahn[1*], Young Kwan Sohn[1], Jin-Young Lee[2] and Jin Cheul Kim[2]

Abstract

Paleomagnetic and rock magnetic investigations were performed on a 64-cm-thick section of nonmarine unconsolidated muddy sediment from the Gosan Formation on Jeju Island, Korea. This sediment was recently dated to have been deposited between 22 and 17 kyr BP calibrated, with a sedimentation rate of 13–25 cm/kyr, based on many radiocarbon ages. Interestingly, stepwise alternating field (AF) demagnetization revealed characteristic natural remanent magnetizations with anomalous directions, manifested by marked deviations from the direction of today's axial dipole field, for some separate depth levels. On the other hand, stepwise thermal (TH) demagnetization showed more complex behavior, resulting in the identification of multiple remanence components. For all TH-treated specimens, consistently two different components are predominant: a low-temperature component unblocked below 240–320 °C entirely having normal-polarity apparently within the secular variation range of the Brunhes Chron, and a high-temperature component with unblocking temperatures (Tubs) between 240–320 and 520–580 °C that have anomalous directions, concentrated in the ~ 13–34-cm-depth interval (~ 17–19 ka in inferred age) and possibly below ~ 53 cm depth (before ~ 20 ka). Rock magnetic results also infer the dominance of low-coercivity magnetic particles having ~ 300 and ~ 580 °C Curie temperature as remanence carriers, suggestive of (titano)maghemite and/or Ti-rich titanomagnetite and magnetite (or Ti-poor titanomagnetite), respectively. A noteworthy finding is that AF demagnetizations in this study often lead to incomplete separation of the two remanence components possibly due to their strongly overlapping AF spectra. The unusual directions do not appear to result from self-reversal remanences. Then, one interpretation is that the low-temperature components are attributable to post-depositional chemical remanences, associated possibly with the later formation of the mineral phase having Tub ~ 300 °C, whereas the high-temperature components are of primary detrital origin that survived later chemical influence. Accordingly, the unusual directions might record geomagnetic instability within the ~ 17–22 ka period manifested by multiple excursional swings, partly associated with the Tianchi/Hilina Pali excursion. However, further work is needed to verify this interpretation and distinguish it from alternative explanations that invoke rock magnetic complexities as the cause of the unusual directions.

Keywords: Gosan formation, Jeju Island, Paleomagnetism, Rock (sediment) magnetism, Geomagnetic instability, Tianchi excursion, Hilina Pali excursion, 17–22 ka period

*Correspondence: mitsuki_ahs@hotmail.com; hs.ahn@gnu.ac.kr
[1] Department of Geology and Research Institute of Natural Science, Gyeongsang National University, Jinju 52828, Republic of Korea
Full list of author information is available at the end of the article

Introduction

Geomagnetic field excursions are short-lived but globally recorded periods of the Earth's magnetic field fluctuation, shorter than a few 10^3 years, during which virtual geomagnetic poles (VGPs) deviate beyond the normal range of secular variation associated with the geocentric axial dipole (GAD) (see Laj and Channell 2007). Paleomagnetic investigations from both lava flow sequences and various types of sediments, especially quasi-continuous deep-sea sediments, in the last two decades have made significant advances in establishing the number, duration and field geometry of geomagnetic excursions, especially during the Quaternary. However, many of them still remain an enigma. Exploring potentially correlative excursions at different sites of the world and increasing their global areal coverage is essential not only to understand how physical processes of the geodynamo modulate frequent occurrence of excursions and what processes discriminate between the geomagnetic reversal and excursion (e.g. Gubbins 1999; Zhang and Gubbins 2000; Hoffman and Singer 2008; Singer et al. 2008), but also to avoid correlation mistakes between temporally different paleomagnetic records from distant sites on the globe (e.g. Laj and Channell 2007; Singer et al. 2008, 2014a; Singer 2014).

Among the geomagnetic excursions that are well documented and proven by numerous studies in the last few decades (e.g. Roberts et al. 2013; Singer 2014), the Mono Lake excursion is the youngest event with an age of ~ 32 ka (Singer, 2014) or ~ 34 ka (Laj et al., 2014) and a duration of less than 2 kyr or about 1 kyr (e.g. Channell 2006; Laj and Channell 2007). As for the period after 30 ka, early paleomagnetic studies reported anomalous field behaviors in direction (or VGP) and/or intensity, with different age populations (see Table 1), speculating that there may be one or more excursion(s) younger than the Laschamp (41 ka in age with a duration of about 1 kyr, e.g. Singer 2014 and Channell et al. 2017) or the Mono Lake excursions, which are the two of well-documented excursions. However, the majority of these previous records were based on limited and/or indirect geochronology and provided equivocal or no direct stratigraphic relationship with the Laschamp and the Mono Lake events, apparently getting skepticism about possible existence of the younger excursion(s). On the other hand, recently documented potential geomagnetic excursions at ~ 17 ka (Singer et al. 2014b) and ~ 26 ka (Channell et al. 2016), based on high-fidelity radiometric chronology or well-constrained age models, as potentially independent excursional events that are also temporally different from the Mono Lake excursion and the Laschamp excursion, suggest a complex picture of geomagnetic field behavior during the post-Mono Lake excursion period.

In addition, some researchers have suggested that such an unusual magnetic field is not always manifested equally at all locations on the globe (e.g. Tarduno et al. 2015). This also emphasizes that paleomagnetic investigation in previously un-investigated regions is always helpful for resolving this issue.

In paleomagnetic studies to identify and characterize such geomagnetic excursions from sediments, a well-established age model, high sedimentation rate (due to the limited duration of geomagnetic excursions), and identification of the magnetic mineralogy in particular are essential. Ferrimagnetic iron sulfides (i.e. greigite, pyrrhotite) and oxidized titanomagnetite (or titanomaghemite) have been often reported as problematic magnetic carriers. Greigite (Fe_3O_4) is widely distributed over the world, found in anoxic and sulfidic sedimentary environments like estuaries, fluvial fans, hemipelagic marines and gas hydrate systems, forming authigenically in reductive diagenetic processes (e.g. Fu et al. 2008; Roberts et al. 2011). It can generate a "false" magnetic record of the geomagnetic fluctuation when the age of greigite formation significantly postdates the age of deposition of the surrounding sediments (e.g. Horng et al. 1998; Jiang et al. 2001; Roberts and Weaver 2005; Sagnotti et al. 2005). Pyrrhotite (Fe_7S_8) often generates such false geomagnetic fluctuations by such late diagenetic formation (e.g. Weaver et al. 2002) or by the self-reversed magnetizations (e.g. Bhimasankaram 1964; Bina and Daly 1994). In addition, some studies on marine sediments suggest that non-steady-state magnetic mineral reductions can result in delayed remanence acquisition leading to anomalous features in natural remanent magnetization (NRM) data (e.g. Tarduno et al. 1996, 1998). Tarduno et al. (1998), for example, suggest that the production of biogenetic magnetite near the Fe-redox boundary at depth can lead to the acquisition of a biochemical remanence. Changes in the redox boundary depth with time in pelagic sediments can result in complexities in magnetic records.

Another complexity can be caused by the presence of titanomaghemite. Titanomaghemite, which is usually formed by low-temperature oxidation (maghemitization) of titanomagnetite in nature, can acquire a partial or complete self-reversed chemical remanent magnetization (CRM) that replaces the original detrital remanent magnetization (DRM) or thermoremanent magnetization (TRM) (e.g. Doubrovine and Tarduno 2004; Krása et al. 2005; Channell and Xuan 2009; Xuan and Channell 2010; Xuan et al. 2012). As a possible mechanism of the self-reversal, ionic reordering (Doubrovine and Tarduno 2004, 2006a) and magnetic coupling between titanomagnetite and oxidized titanomaghemite in a close side-by-side assemblage (Krása et al. 2005) have been suggested. Moreover, observations of self-reversal for

Table 1 Previously reported excursional or anomalous magnetic field behavior during 15–30 ka Modified and added from Singer et al. (2014b)

Ref.	Location	Age (ka)	Chronology	Paleomagnetic features	Remarks
Sediments					
Modern demagnetization and directional analysis used					
Rieck et al. (1992)	Tulelake, California	17–18	tephrochronology, sed. rates	Negative inclination	Younger than 23.4 ka ash bed
Peck et al. (1996)	Lake Baikal, Siberia	19–20	AMS ^{14}C, sed. rate	Large departure of declination and inclination from the GAD direction in several cores	Large uncertainty in C reservoir correction and sed. rates
Nowaczyk et al. (1994), Nowaczyk and Knies (2000), Nowaczyk et al. (2003)	Fram Strait, Arctic Ocean	19–20	AMS ^{14}C	Low (or negative) inclination and low RPI in some	Younger than Laschamp and Mono Lake (Auckland) excursion in same cores
Yamazaki et al. (2003)	northwest off Hokkaido, Japan	25–26	AMS ^{14}C (Itaki and Ikehara, 2003)	Low inclination	Paleodirection on fringe of secular variation
Macrì et al. (2005)	Wilkes Land Basin, Antarctica	15	age model based on RPI correlation	Low inclination and low RPI	The age model was reconstructed by correlation of the RPI records to global reference curves (Guyodo and Valet 1999; Laj et al. 2002a), in agreement with ^{14}C age and biostratigraphic constraints
		24		Low inclination and low RPI	
Hayashida et al. (2007)	Lake Biwa, Japan	27	age model based on tephrochronology and AMS ^{14}C calibrated	Low inclination	Paleodirection on fringe of secular variation; younger than the Aira-Tn (c. 28.8 ka) ash layer
Xuan et al. (2012)	Yermak Plateau (Core 22), Arctic Ocean	17–18	d^{18}O correlation with AMS ^{14}C calibrated	Low inclination	
Lisé-Pronovost et al. (2013)	Laguna Potrok Aike, southern Argentina	20	AMS ^{14}C calibrated	Slightly low inclination and low RPI	Paleodirection on fringe of secular variation
Channell et al. (2016)	Rockall Trough, NE Atlantic	26.5	AMS ^{14}C calibrated, d^{18}O correlation	Reversed paleodirection and RPI minimum	Duration of c. 350 yrs; younger than Laschamp and Mono Lake (Auckland) excursion in same core
Figs. S1 to S3 in Lund et al. (2017)	Bermuda Rise and Blake Outer Ridge, western North Atlantic	19–21	age model based on d^{18}O correlation (to GISP2)	High-amplitude secular variation and RPI minimum	Cores CH89-9P, CH88-10P, and JPC-14
		22–23		High-amplitude secular variation and RPI minimum	
Modern demagnetization and directional analysis not used					
Clark and Kennett (1973)	Gulf of Mexico	12–17	foraminifera, sed. rates	Low inclination in 8 cores	Not found in more recent studies
Yaskawa et al. (1973)	Lake Biwa, Japan	18	^{14}C, sed. rate	VGPs beyond secular variation	not found by Hayashida et al. (2007)
Noltimier and Colinvaux (1976)	Imuruk Lake, Alaska	17–18	^{14}C, sed. rate	Low inclination	Younger than 20 ka but large age uncertainty; possible glacial disturbance of core?

Table 1 continued

Ref.	Location	Age (ka)	Chronology	Paleomagnetic features	Remarks
Lava flows					
Coe et al. (1978)	Hilina Pali, Hawaii	17.8	^{14}C	Low inclination and paleointensity	^{14}C ages were from Rubin and Berthold (1961) and did not directly date the lava flows
Laj et al. (2002b)	SOH4 core, Hawaii	18	age model based ^{14}C ages and geomagnetic tie-points	Negative inclination and low paleointensity	Age model is from Quane et al. (2000); younger than Laschamp and Mono Lake (Auckland) excursion in same core
Teanby et al. (2002)	SOH1 core, Hawaii	20	$^{40}Ar/^{39}Ar$, K–Ar, lava accumulation rate	Negative inclinations and low paleointensities in c. 40 lava flows	Younger than Laschamp and Mono Lake (Auckland) excursion in same core
Cassata et al. (2008)	Hampton Park volcano, Auckland	26.6	$^{40}Ar/^{39}Ar$	Intermediate VGPs (Shibuya et al. 1992) and low paleointensity (Mochizuki et al. 2006)	
Turrin et al. (2013)	Swift Creek, Washington	17.3	$^{40}Ar/^{39}Ar$	Low inclination	Paleodirection on fringe of secular variation
	Tabernacle Hill, Utah	16.9		Low inclination	
Singer et al. (2014b)	Tianchi (Cheonji), China	17.1	$^{40}Ar/^{39}Ar$	Low paleointensity and VGPs with low northern and southern latitudes (Zhu et al. 2000)	
Leonard et al. (2017)	Taylors Hill, Auckland	27.4	$^{40}Ar/^{39}Ar$	Intermediate VGPs (Cassidy 2006)	

titanomaghemites by Doubrovine and Tarduno (2005, 2006a, b) suggest that a finite range of high oxidation states of z (O'reilly 2012) of no less than 0.9 and relatively high Ti contents (x) of no less than 0.6 are required to generate self-reversed remanences.

Here we firstly document a sequence of unusual NRM data, of which the directions deviate visually from the apparent secular variation range during a stable normal-polarity period, from one site of ~ 17–22 ka unconsolidated nonmarine sediment (named Gosan Formation) in Jeju Island, Korea. This study shows (1) that, from thermal (TH) demagnetizations, the unusual paleomagnetic directions all are from remanence components with an unblocking temperature (Tub) interval ranging from 240–320 to 520–580 °C (probably carried by magnetite or Ti-poor titanomagnetite) which are separate from remanence overprints with Tubs up to 240–320 °C (probably carried by (titano)maghemite and/or Ti–rich titanomagnetite) having directions apparently within the secular variation range of the Brunhes Chron, and (2) that alternating field (AF) demagnetization technique often appears to fail to isolate these two different remanences presumably because of their strongly overlapping coercivity spectra. Hence, we address interpretation of these results about whether the unusual directional features are associated with geomagnetic excursional behavior or rock magnetic anomalies.

Geological background and previous works

Jeju Island, located to the south off the Korean Peninsula, is a Quaternary volcanic field formed in an intraplate tectonic setting on the eastern continental margin of the Eurasian plate (Fig. 1a). The island was generated by extensive hydrovolcanism between c. 1.8 and 0.5 Ma and later plateau- and shield-forming, basaltic-to-trachytic lava effusions that produced a wide and low-altitude lava plateau and a peak of shield volcano (Mt. Halla) dotted with hundreds of monogenetic volcanic scoria cones and tuff rings/cones (e.g. Sohn and Park 2004; Sohn et al. 2008; Koh et al. 2013). Besides, paleosols, lake or wetland sediments, and other unspecified, unconsolidated sediments are often observed between or on the top of such volcanic deposits in the island (e.g. Park et al. 1998, 2000a, b; Lee et al. 2014a, b; Park et al. 2014; Lim et al. 2015; Ahn and Choi 2016).

The Gosan Formation (GSF) is a muddy sedimentary formation, a few meters thick and massive, intercalated between the Late Pleistocene plateau-forming basaltic lava, named the Kwanghaeak Basalt, and the basaltic tuff of the Suwolbong tuff ring (Sohn and Chough 1989). The GSF was dated to be approximately 18 ka by optical stimulated luminescence (OSL) method (Cheong et al. 2007). The GSF is exposed approximately 4.5 km along the western coast of Jeju Island, and extending ~ 2 km landward and used as a rice field at present (Park et al. 2000a; Fig. 1b). The main source of the GSF sediment was Dangsanbong, which is a 450 kyr-old, horseshoe-shaped tuff cone with a nested scoria cone at its center (Sohn and Park 2005; Brenna et al. 2015). The stratigraphic relationship near Dangsanbong suggests that the tuff cone was overlain by the Kwanghaeak Basalt after the cone was lithified and significantly eroded (e.g. Park et al. 2000a). Dangsanbong continued to supply volcaniclastic materials to nearby areas, forming a scree deposit upon the basalt. The GSF muddy sediment is laterally correlative with the Dangsanbong-derived scree deposit and thins and pinches out toward the south, i.e., away from Dangsanbong. The sediment is massive and has a fairly level upper surface without any features related to fluvial incision, wave reworking or bioturbation. It is therefore interpreted to have been deposited by suspension setting of fines in a wetland near the toe of the scree that surrounds Dangsanbong.

OSL age of the GSF was obtained earlier by Cheong et al. (2007) and was estimated at 23.2 ± 1.0 ka. Afterward, a research group of the Korea Institute of Geoscience and Mineral Resources (KIGAM) carried out more detailed, absolute age dating and geochemical analyses over a wider area of the GSF exposures (Lee et al. 2014b). Part of these results including a suite of radiocarbon (^{14}C) ages with an accelerator mass spectrometry (AMS), granulometry, contents of total organic carbon (TOC) and its $\delta^{13}C$ ($=^{13}C/^{12}C$) ratios for a site at the coast near Dangsanbong (hereafter referred to as site GSDS; see Fig. 1B) were published in Lim et al. (2015). Median grain sizes for the GSDS site varied between ca. 12 and 18 μm, having an apparently consistent value around 15 μm. The TOC contents ranging between 2.0 and 0.8% (totally low throughout the sediment) monotonously decrease with depth. In combination with the AMS ^{14}C ages, they suggested that the GSF sediment was deposited in a terrestrial (and probably subaqueous) environment during a period approximately between 22 and 17 calibrated (cal.) kyr BP (Fig. 2 and Additional file 1: Table S1), and that the age of the Suwolbong tuff ring should be younger than the previous estimate (~ 18 ka; Cheong et al. 2007). Lee et al. (2014b)'s work at another GSF site near Suwolbong (hereafter referred to as GSSW; see Fig. 1b) has also yielded a line of AMS ^{14}C dates, suggesting a wide range of the GSF sedimentation age from 24 to 16 cal. kyr BP (Fig. 2 and Additional file 1: Table S1). Age-depth model for each site was made by linear interpolations between AMS ^{14}C age estimates, as shown in Fig. 2. The GSSW and GSDS age-depth models were similar for, at least, the upper ca. 70 cm sediments, where the estimated sedimentation rates are much higher than

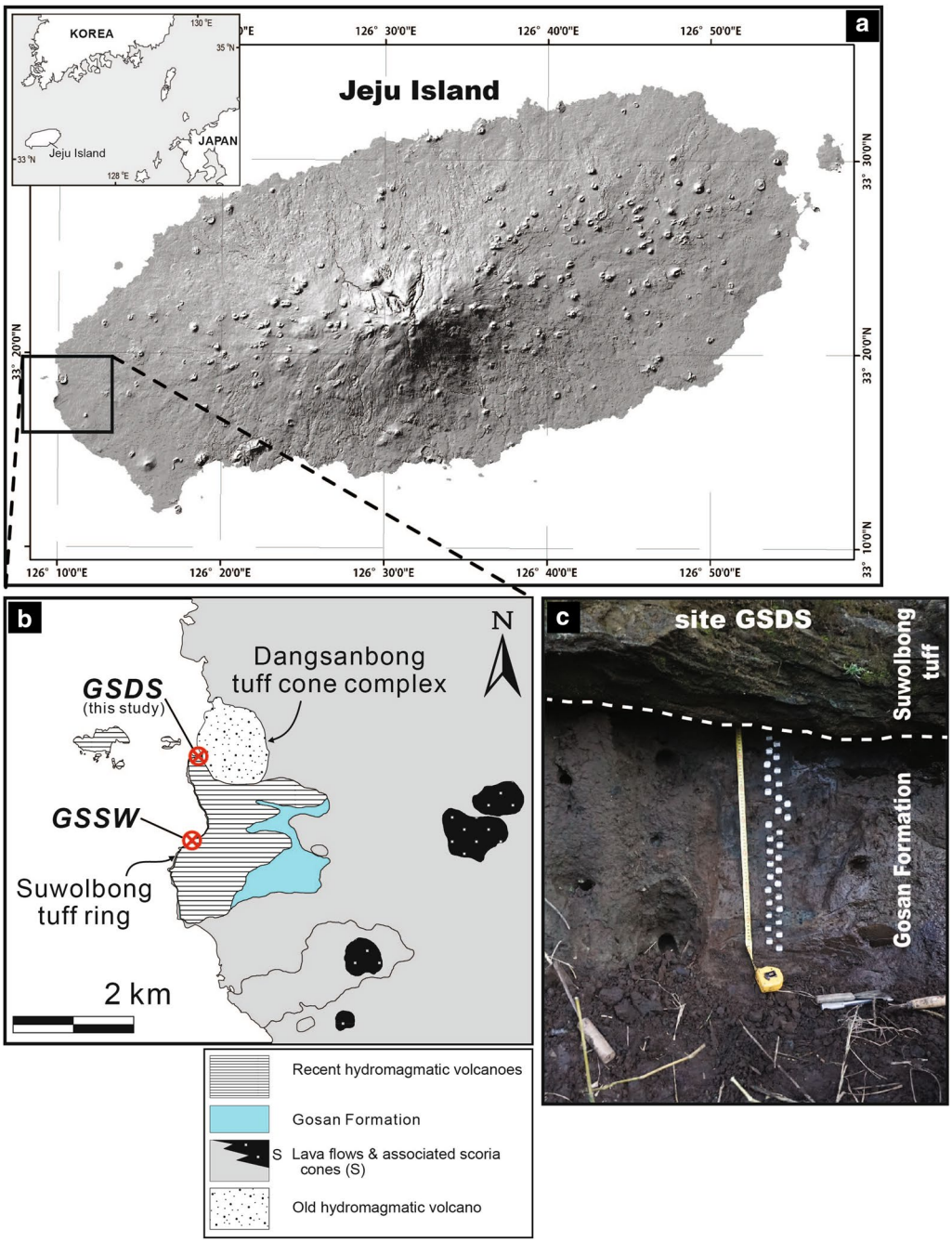

Fig. 1 **a** Digital elevation model of Jeju Island (the location is indicated in the insert), showing a 1950-m-high central peak (Mt. Hallasan) at the center of a gently sloping and broadly distributed lava shield, dotted with hundreds of volcanic cones, rings and domes. **b** Geologic map around the western coast of Jeju Island, including the Suwolbong tuff ring, the Dangsanbong tuff cone complex, and Gosan Formation (modified from Park et al. 2000a), with the locations of studied sites in Gosan Formation (GSDS, this study; GSSW, Lee et al. 2014b). **c** Paleomagnetic sampling of the GSDS section (during the first field campaign)

10 cm/kyr (in the range of 13–25 cm/kyr). The above-mentioned age data with related additional information are also listed in Additional file 1: Table S1.

Samples and methods

We made paleomagnetic sampling at the same site analyzed in Lim et al. (2015) (i.e. site GSDS, 33.30917°N, 126.16556°E; Fig. 1b). The site GSDS was found to be

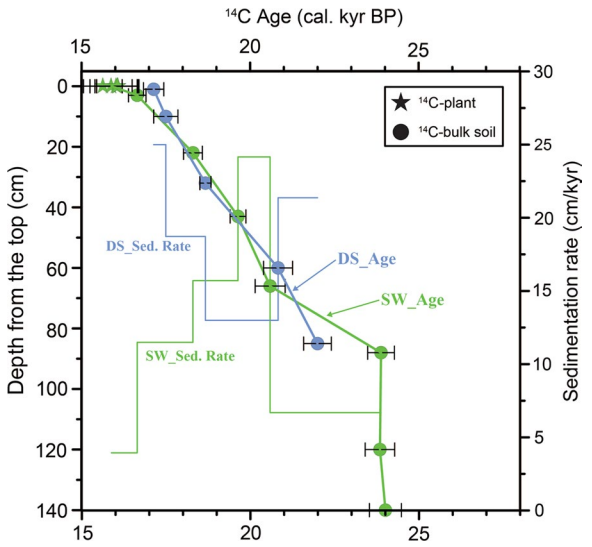

Fig. 2 Age-depth models and associated sedimentation rates in two sites of the Gosan Formation sediments (blue, site GSDS; green, site GSSW), on the basis of AMS radiocarbon (^{14}C) dates (Lee et al. 2014b; Lim et al. 2015). The ^{14}C dates (with the 2σ error bars) indicated as the tie-points with circle and star symbols were measured on organic materials extracted from bulk soils, and on plant remains, respectively, and were calibrated using the OxCal program (http://c14.arch.ox.ac.uk/embed.php?File=oxcal.html). Note that the sedimentation rates at the 88–140 cm interval in the site GSSW were not drawn

lithologically homogeneous, comprising dark-brown, unconsolidated and massive clayey silt deposit with scattered gravel-sized clasts. The estimated sedimentation rate varying between 13 and 25 cm/kyr (the blue thin line in Fig. 2) is high enough to record such "short-lived" geomagnetic events. After removing more than 10 cm of surface soils to avoid possible adverse effects of post-deposition alteration and making a planar face, a total of 33 oriented samples were collected at 2-cm-spacing between 5 and 69 cm depths from the top (i.e. from the contact with the Suwolbong tuff), carefully pushing 7 cm^3 non-magnetic plastic cubes into the face and orientating with a magnetic compass with an attachment allowing to mount the plane to be measured (Fig. 1c).

In the laboratories, paleomagnetic and rock magnetic measurements of 33 cube samples were performed as follows.

[1] Stepwise alternating field demagnetization (SAFD) of NRM,
[2] SAFD of laboratory-induced anhysteretic remanent magnetization (ARM),
[3] Isothermal remanence (IRM) acquisitions in direct current (DC) fields of sequentially 1 T, −0.1 and −0.3 T,
[4] Initial magnetic susceptibilities with dual frequencies (k_{LF} and k_{HF}), then for each of three sets of small-volume (< 0.1 g) dried subsamples from selected samples,
[5] Thermomagnetic analysis of saturation magnetization (*Js*–*T* curve),
[6] Thermomagnetic analysis of magnetic susceptibility (*k*–*T* curve),
[7] Measurements of magnetic hysteresis properties (Mrs, saturation remanent magnetization; Ms, saturation magnetization; Bcr, coercivity of remanence; Bc, coercive force),
[8] First-order reversal curve (FORC) analysis (e.g. Roberts et al. 2000), then finally, for each of cube-shaped preparations that were consolidated with plaster and wrapped in Al-foil after extracting form each of selected samples,
[9] Stepwise thermal demagnetization (STHD) of 3-axis IRMs imposed sequentially in DC fields of 1.2, 0.4 and 0.1 T (the Lowrie experiment following the procedure of Lowrie 1990).

Experimental sequences [1]–[5] and [9] were carried out at the paleomagnetism and rock magnetism laboratory of the Center for Advanced Marine Core Research (CMCR) of Kochi University in Japan, and sequences [6] and [7] to [8] were performed at the paleomagnetic laboratories of Pusan National University and KIGAM in Korea, respectively.

The remanence measurement, AF demagnetization, ARM acquisition were made using a 2G Enterprises 760R pass-through cryogenic magnetometer with in-line 3-axis static AF demagnetization and ARM acquisition. The SAFD experiments of remanent magnetizations (NRMs and ARMs) were made in generally 23 steps of peak AFs from 0 to 80 mT (the increments of 2 mT for the 0–20 mT peak AFs and 5 mT for the 20–80 mT peak AFs). The ARM acquisitions were imposed in a DC field of 0.1 mT and AF field decaying from a peak AF of 80 mT (k_{ARM} can be calculated following e.g. Banerjee et al. 1981). The IRMs for each bulk cube-shaped sample were acquired using a Magnetic Measurements MMPM10 pulse field magnetizer. The dual k_{LF} and k_{HF} were measured at AF external fields with frequencies of 0.47 and 4.7 kHz, respectively, using a Bartington MS2-MS2B magnetic susceptibility system. The thermomagnetic analysis of saturation magnetization was made by a single heating–cooling run between room temperature and 700 °C with a constant field of 0.3 T and a heating rate of ~ 15 °C/min in air, using a Natsuhara Giken NMB-89 magnetic balance. The thermomagnetic analysis of magnetic susceptibility was conducted, heating from room temperature up to 700 °C and then cooling down to 40 °C,

at 300 A/m field and a heating rate of ~ 12 °C/min in air, using an AGICO KLY-4 Kappabridge system equipped with a CS-3 furnace. The magnetic hysteresis loop and the stepwise back-field IRM demagnetization were measured on each small-volume subsample, applying fields up to 1 T, by means of a Princeton Measurements Corporation MicroMag 3900 alternating gradient magnetometer (AGM). With the AGM, 170 FORCs were also measured on the same subsamples, at averaging time of 200 ms and a field increment of 1.06 mT up to a maximum applied field of 1 T. During the Lowrie experiments, TH demagnetization experiments were performed, using a Natsuhara Giken TDE-91 thermal demagnetizer (residual field of < 15 nT), by measuring the remanent magnetization before every TH step, using a Natsuhara Giken SMD-88 spinner magnetometer. The TH steps were set to 100, 160, 200, 260, 300, 320, 340, 360, 400, 440, 480, 520, 580, 620, 650, and 680 °C (16 steps).

S ratios, $S_{-0.1T}$ and $S_{-0.3T}$, were calculated following the definition of Bloemendal et al. (1992), to seek the relative fraction of low-coercivity minerals with respect to high-coercivity minerals: $S_{-0.1T} = (1 - IRM_{-0.1T}/IRM_{1T})/2$, and $S_{-0.3T} = (1 - IRM_{-0.3T}/IRM_{1T})/2$, where IRM_{1T} is hereto regarded as saturated IRM (SIRM). Median destructive field (MDF) with respect to each laboratory-induced ARM during SAFD was calculated to see a magnetic hardness to the remanence in relation to coercivity and average grain size of the magnetic minerals. With k_{LF} and k_{HF} values, k_{FD} was calculated as k_{FD} (%) $= (k_{LF} - k_{HF})/k_{LF} * 100$, to see the possible contribution of superparamagnetic (SP; < 50 nm in general) minerals (e.g. Evans and Heller 2003). k_{ARM}/SIRM, k_{ARM}/k_{LF}, and SIRM/k_{LF} ratios for bulk samples were employed as a proxy of grain-size fluctuations in relation to the domain state of magnetic particles (e.g. Banerjee et al. 1981). The SIRM/k_{LF} ratio can be also used as indicator of the dominance of greigite (e.g. Roberts et al. 2011; Nowaczyk et al. 2012). The hysteresis parameters were processed with a biplot of the Mrs/Ms ratio versus the Bcr/Bc ratio (so-called "Day plot" from Day et al. 1977), to obtain information about the average grain-size of magnetic particles. The measured FORCs were processed with the FORCinel software (Harrison and Feinberg 2008) to display a FORC diagrams, which provide information about distributions on microscale coercivity and magnetostatic interaction. The experiments [5], [6] and [10] give information about the contained magnetic minerals. As introduced by Peters and Thompson (1998), the two biplots of SIRM/k_{LF} versus $ARM_{dem40mT}$/ARM and $IRM_{-0.1T}$/SIRM versus $ARM_{dem40mT}$/ARM, where $ARM_{dem40mT}$ denotes the ARM intensity after demagnetization by a peak AF 40 mT, were employed to discriminate magnetic minerals with low coercivities.

Afterward, another set of three oriented block samples with plastic boxes of ca. 13 cm × 18 cm × 4 cm in size were also collected from a 5-to-55-cm-depth profile in close proximity of the "first-sampled" point in the GSDS site. The block samples, in the laboratory, were consolidated with plaster and cut to cube-shaped specimens with 2 or 2.2 cm on each side. Two pairs of Al-foil wrapped cubes for 21 successive depth levels (7.1–50 cm depths in the central position) were then prepared to make STHD and SAFD experiments for NRM, respectively. Central depth levels of the prepared cube-cut specimens from three blocks were 7.1–20.3, 23.1–36.3, and 38.0–50.0 cm, respectively. The STHD experiment of NRM was treated in 40 °C steps in the 120–580 °C range and in 20 °C steps in the 580–640 (660) °C range. The SAFD experiment of NRM was same as in the earlier AF treatments. The specimens with AF treatments and NRM measurements were then subjected to ARM acquisition followed by its SAFD experiment.

Compass readings of the sample orientation were corrected for the locality declination of the present-day Earth's magnetic field of 7°, calculated using the 12th International Geomagnetic Reference Field (Thébault et al. 2015; http://wdc.kugi.kyoto-u.ac.jp/igrf/point/index-j.html). Demagnetization data were identified with the orthogonal vector diagram of Zijderveld (1967) and equal-area projection. Principal component analysis (PCA) of remanent magnetization for each demagnetization data was performed applying Kirschvink (1980). Mean direction for the isolated remanence components was calculated using a Fisherian statistics (Fisher 1953).

Results and discussion

Paleomagnetic results

Results on "first-sampled" specimens

Initial NRM intensities in "first-sampled" specimens (labeled here as "GSDS1-*xx*cm-AF") were mostly in the order of 0.01 A/m with a minor variation but three occasional exceptions of larger than 0.1 A/m in specimens from 9, 21 and 39 cm depths from the top (Additional file 1: Table S2).

NRM-SAFD experiments revealed that remanent magnetization for each of most analyzed samples was identified by one or two directional components after soft demagnetizations up to 2–10 mT in peak AF which is probably associated with recently induced remanence during or after sampling (for example, 0–4 mT AFs for specimen GSDS1–27 cm-AF in Fig. 3; named here as LFC0). Then demagnetization patterns could be classified into six types as shown in Fig. 3. Type IA (Fig. 3a), which was found in 9 samples, could be characterized by a single magnetic component decaying toward the origin after removal of the soft remanence (LFC0). This

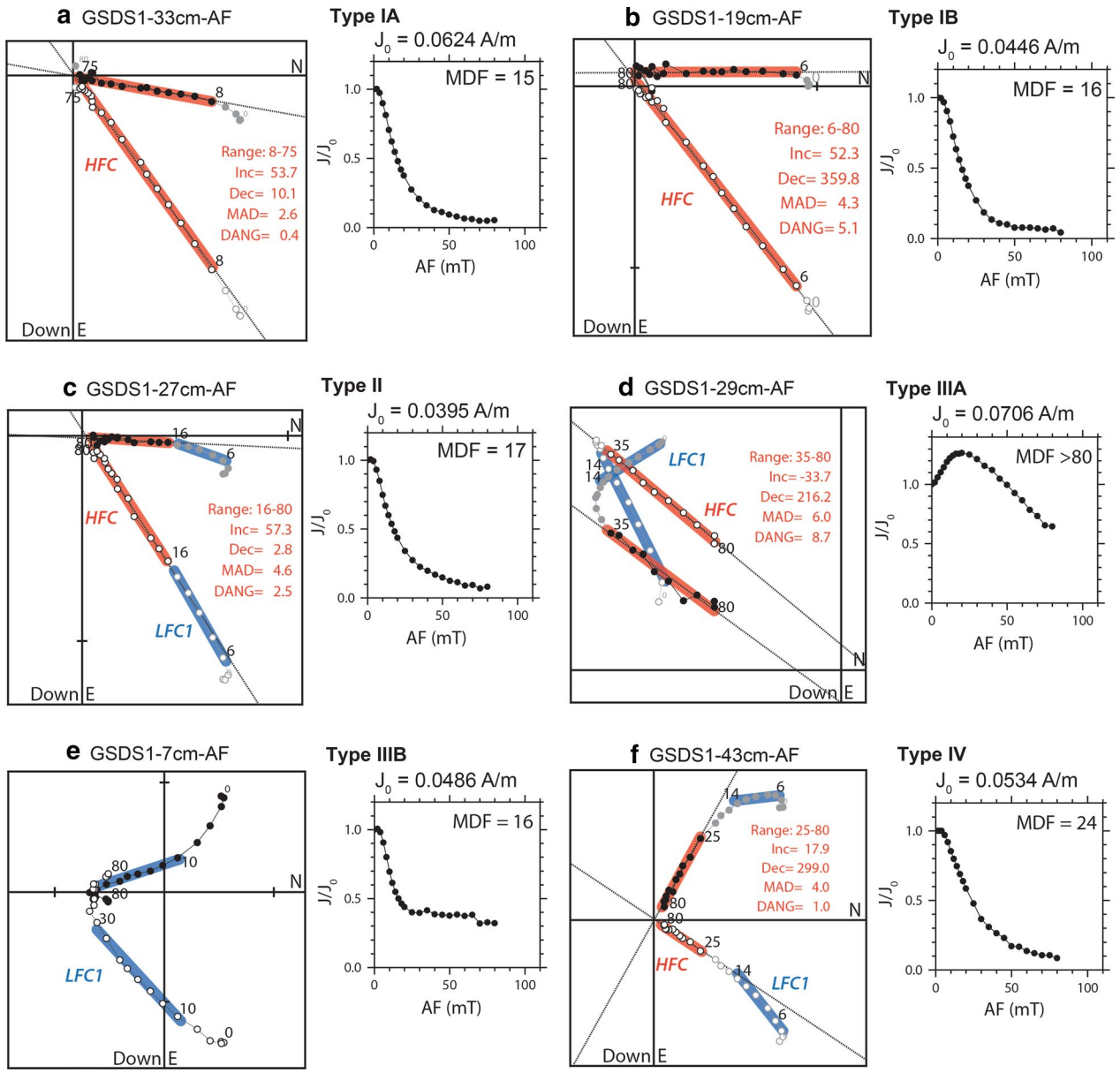

Fig. 3 Typical stepwise AF demagnetization results of NRMs for the first-sampled (GSDS1) specimens, individually displayed on the orthogonal vector diagram (Zijderveld 1967), illustrating the HFC (red bar) and LFC1 (blue bar) segments (see text for details), with the associated NRM intensity decay curve. A characteristic (HFC) direction determined by the PCA (Kirschvink 1980) without anchoring the origin is shown. On the Zijderveld diagram, open (closed) dots indicate the end-points of NRM vectors in the vertical (horizontal) plane at each AF level. For details of the respective types of the results, **a** to **f**, see text ("Paleomagnetic results" section)

single component indicated a normal-polarity direction. One specimen, GSDS1–19 cm-AF (Fig. 3b), had a similar pattern as type IA but the defined single component did not seem to direct to the origin (type IB). Other 11 samples had two directional components, of which the high-coercivity one could not be recognized unless AF demagnetization persists up to > 10–30 mT and had a normal-polarity direction. Note that in several specimens of this case the high-coercivity component had unstable in some degree and/or did not appear to direct to the origin. This kind of the patterns corresponded to type II (Fig. 3c). Both types IIIA (Fig. 3d) and IIIB (Fig. 3e) could be characterized by a high-coercivity component with reverse-polarity directions, separate from normal-magnetized overprint not to anti-parallel to each other, was visible or seemed to be. Two samples of type

IIIA (29 and 65 cm depth) displayed apparently a stable high-coercivity component, whereas other two with type IIIB (7 and 17 cm depth) did indicate incomplete isolation of the reverse-polarity magnetization from the overprint. There were five results showing two different components, in which the high-coercivity one could be defined by AF demagnetizations above 25 mT at least and appeared to be intermediate-polarity magnetized (type IV; Fig. 3f). Two remaining results (23 and 63) were unclassified because the demagnetization behavior above the 10–18 mT AF steps was chaotic.

For all analyzed samples, MDF values during the SAFD of NRM were in the limited range of 10–29 mT, but for 29, 39 and 65 cm depth levels that have much higher MDFs.

Low-coercivity remanence component defined in AF steps between 2–10 and up to 35 mT (LFC1), where visible, had a direction being scattered around the GAD-expected direction ($D = 0°$, $I = 53°$), as seen in Fig. 3c–f. On the other hand, high-coercivity remanence component (HFC) was generally defined in AF intervals including peak fields above ~ 35 mT by applying the PCA without anchoring the origin, having a maximum angular deviation (MAD) value smaller than 15°, for 27 out of 33 specimens analyzed. This non-anchoring-determined HFC generally had no significant difference from the anchoring-derived direction at the same AF interval (hereafter called "DANG") by less than 5°, except for 8 specimens (for example, DANG = 8.7° in Fig. 3d) (see also Additional file 1: Table S3). More importantly, there were unusual HFC directions (for the 5,9, 29, 43 and 65 cm depth levels) apart largely from the GAD direction (in other words, low latitudes in corresponding VGP, more than ~ 45° away from the North Pole), besides normal-polarity HFC directions within the apparent secular variation range of the Brunhes Chron.

Results on "second-sampled" specimens

Twenty-one pairs of adhering specimens for the 7.1-cm-to-50-cm-depth "second-sampled" profile (labeled here as "GSDS2-*xx.x*cm-AF/TH") yielded paired STHD and SAFD results of NRMs for the same depth levels. It is found that TH demagnetization behavior was more complex, compared to AF one, in many of them. Figure 4 shows three pairs of TH and AF results. These TH results recognized generally three but four, in maximum, different directional components as follows:

(1) the lowest temperature component determined in the room temperature (20 °C)–120 °C range (LTC0),
(2) the low-temperature component determined in TH steps between 120 and 240–320 °C (LTC1),
(3) the high-temperature component determined in TH steps between 240–320 and 520–580 °C (HTC1), and
(4) the highest temperature component determined in TH steps between 520–580 and 620–660 °C (HTC2).

The LTC0, having dominantly a direction with $D \sim 10°$–$50°$ and $I \sim 120°$–$170°$, was considered as viscous remanences induced during the sampling and/or the storage. This corresponded to the lowest component with AFs up to 4–8 mT (LFC0) in the AF result. The LTC1 directions all were around the GAD direction (apparently within the secular variation range of a stable normal-polarity period). This appeared to correspond to the low-coercivity component with the AF steps between 6–10 and 30 mT or higher (LFC1). On the other hand, The HTC1 direction had highly varied directions, in which some were reversed and intermediate-magnetized. This HTC1 direction was not often apparent in the AF demagnetization result, as shown in Fig. 4. The HTC2 component (for example, 7.1 cm in Fig. 4) was found only in some depth levels, of which seven could define the HTC2 which had directions with northerly declinations and shallow positive inclinations. Our demagnetization results indicate that AF demagnetizations often resulted in incomplete isolation of remanence components corresponding to the TH-derived high-temperature ones, such as HTC1 and HTC2, being screened by a large portion of the low-coercivity components (LTC0 and/or LTC1). These LTC1, HTC1 and HTC2 direction data are also listed in Additional file 1: Table S4.

Additionally, there were two particular specimens (13.7 and 15.9 cm depth) where NRMs did not decay toward the origin during heating up to 520–560 °C and the NRMs above the 580 °C step were highly unstable, but their directions were apparently anti-parallel to the NRM directions for the 320–560 °C range (HTC1) (Fig. 5).

Rock magnetic analyses

Magnetic properties for k, ARM and IRM

Magnetic susceptibility (k), k_{ARM}, and SIRM are often used as a primary indicator of concentration of magnetic minerals. k_{LF} and k_{ARM} showed a similar variation characterized by relatively large amplitudes in fluctuation and slightly high mean values above 30 cm depth, whereas the lower 40 cm interval represented low values than their averages with a suppressed fluctuation but a slight increasing trend with increasing depth (Fig. 6a, b). SIRM variation broadly resembled those of k_{LF} and k_{ARM}, but it had impressively high peaks in the value at 7–9, 17, 29, 39, and 65 cm depth levels (Fig. 6c). Of these, the 39 and 65 cm peaks did have common k_{LF} and k_{ARM} variations, suggesting that these peaks might have been affected dominantly by an additional magnetic mineral rather

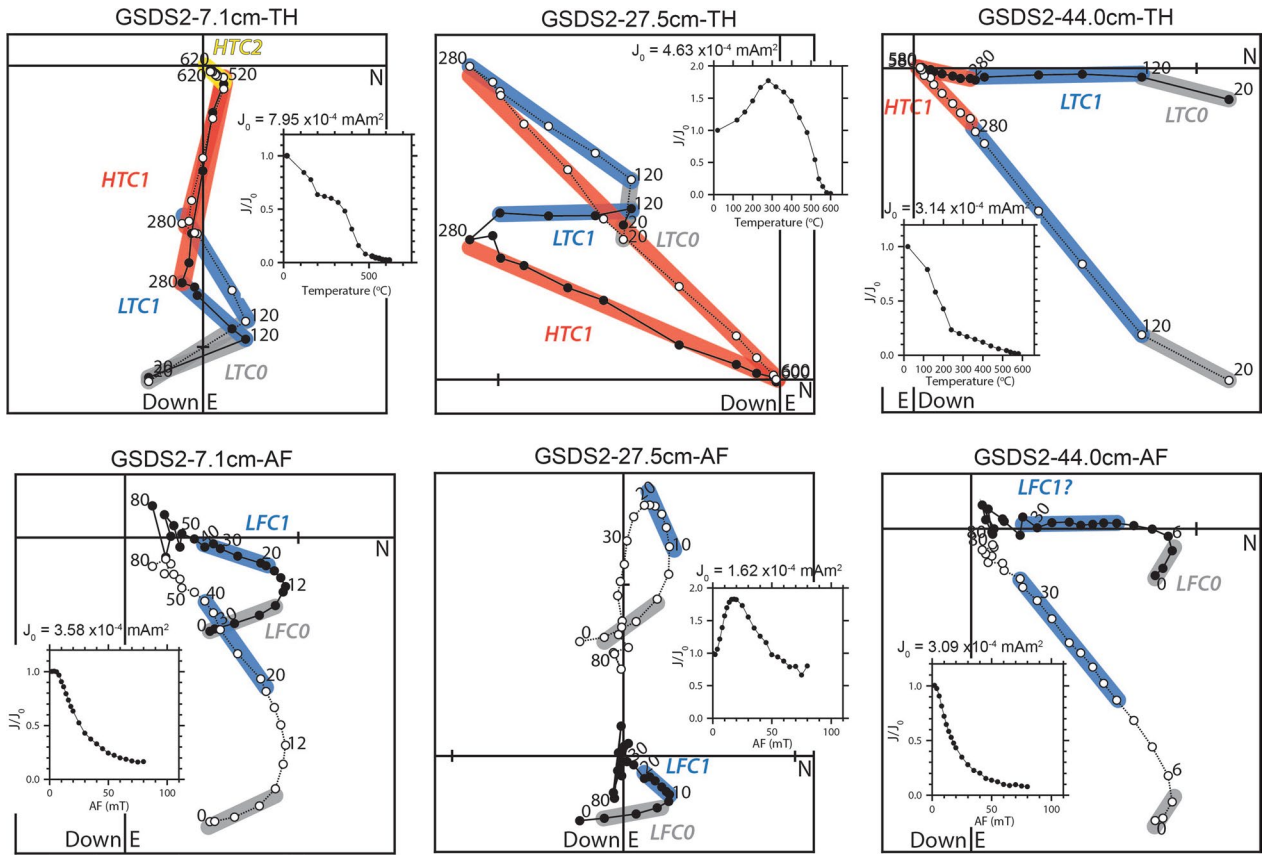

Fig. 4 Zijderveld diagrams and intensity decay curves of stepwise TH demagnetization results for three horizons (7.1, 27.5 and 44.0 cm depth levels; 8.2, 29.0 and 49.0 cmcd, respectively. See text for the definition of cmcd) sampled during the second sampling (GSDS2), compared to those of stepwise AF demagnetization result for adjacent specimens from the same depth level. On the Zijderveld diagrams, the LTC0, LTC1, HTC1 and HTC2 segments for TH-treated results are illustrated with gray, blue, red, yellow bars, respectively, and LFC0 and LFC1 segments for AF-treated results are illustrated with gray and blue, respectively. Other symbols on the Zijderveld diagram are same as in Fig. 3

than the concentration. Variations in k_{ARM}/k_{LF}, k_{ARM}/SIRM, and SIRM/k_{LF} did not appear to show a similarity between them (Fig. 6d–f), in accordance with the possible effect of an additional magnetic mineral. Rather, the SIRM/k_{LF} variation was analogous to the MDF of ARM during AF demagnetization (MDF_{ARM}), showing remarkably high peaks in their values at 39 and 65 cm depth, and apparently 7 cm depth (Fig. 6f–g). While most of the SIRM/k_{LF} values were between 9 and 13 kA/m, for the peak intervals the values were indicated by up to 35 kA/m. Such high peaks in SIRM/k_{LF} (and MDF_{ARM}) may indicate relative abundance of, for example, greigite or other kind of minerals with slightly higher coercivities. The $S_{-0.3T}$ values were as high as 0.98 and most of the $S_{-0.1T}$ values are around 0.90, showing the dominance of low-coercivity minerals throughout the samples (Fig. 6h). However, at 7, 17, 23, 39–41, and 65 cm depth levels, there were relatively low $S_{-0.1T}$ values varying between 0.71 and 0.85, inferring relative abundance of higher coercivity magnetic particles.

Magnetic mineralogy

Figure 7 shows the results of k–T curve, Ms–T curve, and Lowrie experiment for four samples at different depth levels (7, 29, 33, 39 cm) in the "first-sampled" (GSDS1) profile. In all k–t heating curves (Fig. 7a) k increases up to about 300 °C and subsequent decrease was visible and followed by a significant drop at temperatures between 500–570 and 590 °C. The decrease at above ~ 300 °C was occasionally followed by the abrupt increasing between 470 and 550 °C (hump-forming) that were seen for the 33 and 39 cm depth levels. During cooling, there was strong enhancement in k for all cases. Ms–T curves (Fig. 7b) during heating displayed, in addition to a minor inflection at ~ 100 °C, a gradual decrease below ~ 400 °C and subsequent hump-forming approximately between 400 and 500 °C, with a final inflection temperature of ~ 550 °C. The cooling curves did not appear strong enhancement in Ms. In the k and Ms heating curves, the drop approximately between 300 and 400 °C and the hump-like form seen in some samples can infer either

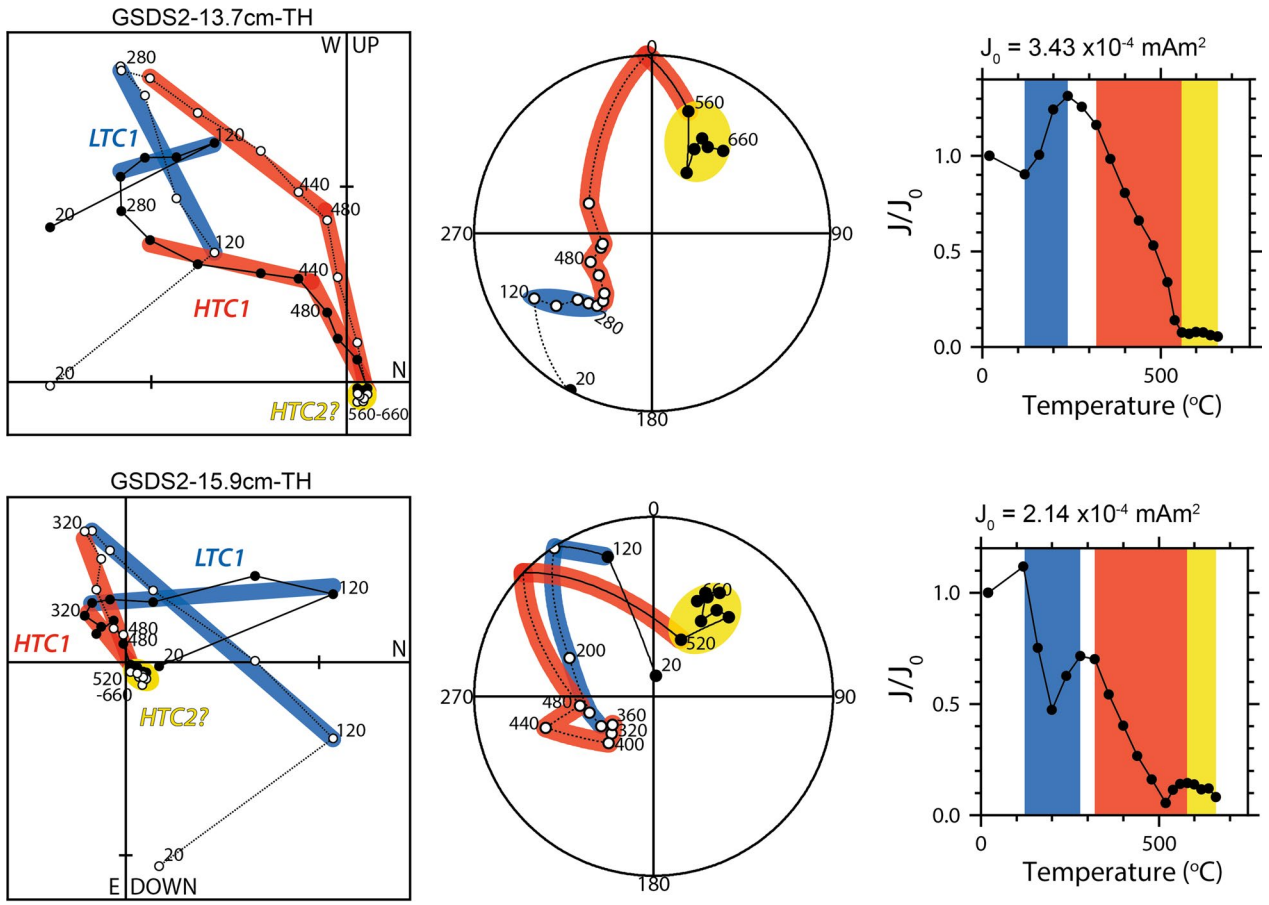

Fig. 5 Zijderveld diagrams (left), equal-area projections (middle), and intensity decay curves (right) of TH demagnetization results of NRMs for two specimens (13.7 and 15.9 cm depth of the GSDS2 profile; 14.8 and 17.0 cmcd, respectively (see text for the cmcd definition)) showing apparently anti-parallel directions between remanences before and above ~ 520–560 °C (see text for details)

exsolution of titanomagnetite to magnetite and ilmenite (e.g. Özdemir 1987), or inversion of (titano)maghemite to magnetite (e.g. Özdemir 1987), or inversion of (ferrimagnetic) iron sulfides to magnetite (e.g. Roberts et al. 2011). The difference between the k–T and Ms–T cooling curves might be associated with the degree of the initial oxidation of samples and/or laboratory conditions during heating, which may cause the inversion partly to hematite upon heating of the Ms–T analysis leading to no remarkable increase during cooling. Lowrie experiments (Fig. 7c) gave us more direct and evident information regarding the remanence carrier. In general, for all analyzed samples IRMs were dominated by low-coercivity (magnetically soft; 0–0.1 T) contribution and they did not have Tubs above 600 °C for all spectra of the coercivities (0–1.2 T). For the 7 and 39 cm samples, more or less medium (0.1–0.4 T) and hard (0.4–1.2 T) components were visible. Both the soft and medium components represented two tubs of 300 and 580 °C, respectively, indicating the co-existence of another "low-to-middle coercivities" magnetic phase with Tub of 300 °C with magnetite (the Curie temperature, Tc ~ 580 °C) as the remanence carrier. The demagnetization behavior of the small hard (0.4–1.2 T) component differed from sample to sample: The 7 cm sample had two Tubs of 300 and 580 °C, and only 580 °C for the 29 cm, only 300 °C for the 39 cm, and none for the 33 cm depth level. The presence of the hard Tub ~ 300 °C magnetic phase (7, 39 cm depth) appeared to be correlated to the $S_{-0.1T}$ lows (Fig. 6h).

In addition, Fig. 8 shows two biplots of SIRM/k_{LF} versus $ARM_{dem40mT}$/ARM, and $IRM_{-0.1T}$/SIRM versus $ARM_{dem40mT}$/ARM, as introduced by Peters and Thompson (1998), which allowed us to discriminate ferrimagnetic iron oxides from ferrimagnetic iron sulfides among "low-coercivity" magnetic minerals. These indicate no presence of greigite and pyrrhotite. Also, no presence of greigite could be supported by the following data: (1) extremely low values (nearly zero or 0.06 at most) in gyroremanent magnetization (GRM) index (GI), which is a measure to quantify the potential GRM effect by

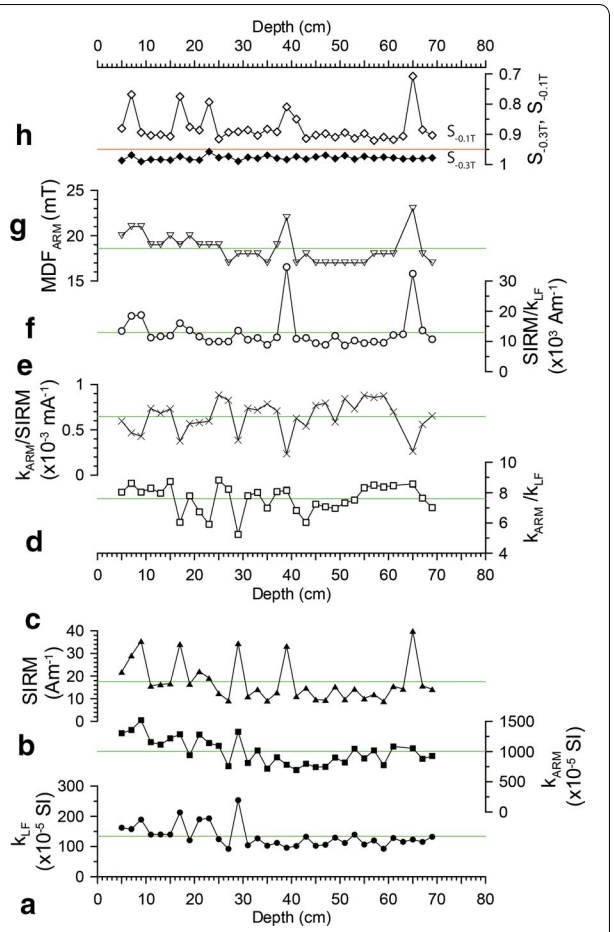

Fig. 6 Variations, as a function of depth, in some bulk rock magnetic parameters from the GSDS1 profile, **a** k_{LF}, **b** k_{ARM}, **c** SIRM, **d** k_{ARM}/k_{LF} ratio, **e** k_{ARM}/SIRM ratio, **f** SIRM/k_{LF} ratio, **g** MDF_{ARM}, and **h** *S* ratios ($S_{-0.1T}$ and $S_{-0.3T}$). Green bar for each of Fig. 5a–g denotes the individual average values. Values of these parameters are also listed in Additional file 1: Table S3

greigite and is calculated as the ratio of the difference between the intensity value at the highest demagnetization level (80 mT hereto, J80 mT) and the minimum intensity reached during demagnetization (*J*min) and the difference between the initial value (*J*0) and the same minimum in intensity, GI = [*J*80 mT − *J*min]/[*J*0 − *J*min] (Fu et al. 2008), with respect to the NRMs, and (2) absence of FORC maxima above about 40 mT in Bc with considerable magnetostatic interaction (e.g. Roberts et al. 2000; Rowan and Roberts 2006; see Fig. 10b), and by much lower than about 40 mT in Bcr (Roberts et al. 2011 and references cited therein; see Fig. 9). Furthermore, there were some cases for the TH demagnetization where NRM intensity persisted by larger than 10% of the total even after demagnetization at 580 °C and the remaining NRM appeared to be fully demagnetized by heating to ~ 620 °C or higher (7.1, 20.3, 23.1, 25.3, 29.7, 34.1, and 36.3 cm depth in the GSDS2 profile). Given the observation of the $S_{-0.3T}$ ratios near saturation (Fig. 6h), this may imply a possibility of some presence of maghemite with thermal stability, apparently consistent with the previous studies showing the possible high-temperature Curie temperature and its stability by up to approximately 645 °C of maghemite (e.g. Özdemir and Banerjee 1984; Gehring et al. 2009).

Therefore, it is possible to interpret that in the entire sediment, besides magnetite (or Ti-poor titanomagnetite), a magnetic phase of ~ 300 °C in Tc with a different range of coercivities, possibly suggestive of (titano)maghemite or relatively Ti–rich titanomagnetite or both (i.e. partially maghemitized titanomagnetite), is pervasive as the remanence carrier and that occasionally maghemite with high-temperature stability also would be present. Also, it is obvious that these two Tcs (or tubs) identified above are in excellent agreement with the lowest and/or the highest temperatures that discriminate the partial remanence components in the TH demagnetization results for all analyzed specimens.

Magnetic granulometry

Magnetic hysteresis loop and stepwise DC back-field demagnetization of IRM and FORCs were obtained on each of subsamples from selected 8 depth levels (7, 17, 29, 33, 39, 57, 65, and 67 cm depths in the GSDS1 profile). The hysteresis loops after correcting for the paramagnetic contribution using a high-field slope are shown in Fig. 9, and Day plot of the hysteresis parameters is illustrated in Fig. 10a. FORC diagrams for the 7 and 65 cm depth are presented in Fig. 10b.

Analyzed samples all displayed consistently an identical hysteresis loop in the shape which was thinly opened but not "wasp-waisted", characterized as a pseudo-single-domain (PSD) loop (Tauxe 2010), with narrow ranges of 10–12 mT in Bc and 25–28 mT in Bcr (Fig. 9). This is in agreement with the result on the Day plot (Fig. 10a) that define cluster of data points of limited Mrs/Ms (0.21–0.25) and Bcr/Bc (2.3–2.6), falling in the medial leftward side of the PSD region, and close to the theoretical curve 3 for a mixture of single-domain (SD) and multi-domain (MD) particles derived by Dunlop (2002a, b). As shown in Fig. 10b, the FORC diagrams have very similar characteristics that were expressed by remarkable spreading of closed contours along the Bc axis, centered at 10–12 and < 5 mT (SD contributions), and modest-to-little degrees of divergent contours toward the Bu axis (MD contribution) and restricted vertical dispersion (supressed magnetostatic interaction), but no vertical spreading of the contours at Bc = 0 mT along the Bu axis (contribution of SP particles). From these results, granulometry of the magnetic particles could be interpreted as

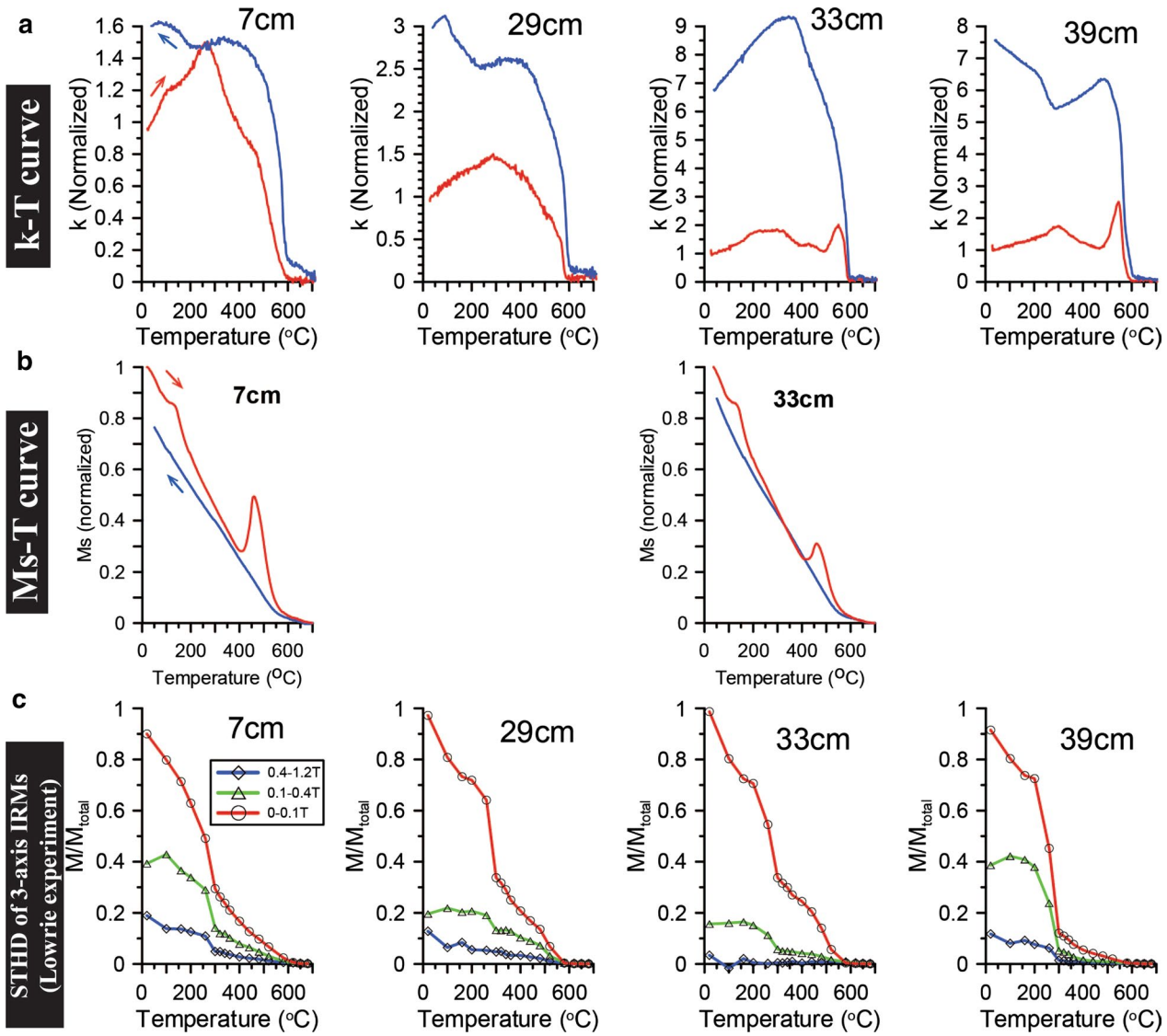

Fig. 7 Results of **a** high-temperature weak-field thermomagnetic (*k*–*T*) curve, **b** high-temperature strong-field thermomagnetic (Ms–*T*) curve, and **c** STHD of 3-axis IRMs with different coercivities (Lowrie 1990), from selected horizons (7, 29, 33 and 39 cm depth of the GSDS1 profile)

a mixture of SD particles with two slightly different mean coercivities and coarser (PSD to possibly less MD) particles, with supressed magnetostatic interaction.

Combining paleomagnetic data

Prior to discussing the origin of unusual NRM directions, it was necessary to check the stratigraphic relationship of two paleomagnetic data sets from between the GSDS1 and the GSDS2 profiles in the GSDS site through comparison between their rock magnetic properties. First, we found that variation pattern in ratio of NRM intensity after TH demagnetization at 580 °C to initial NRM intensity ($NRM_{580°C}/NRM_{20°C}$) of the GSDS2 profile closely mimic the $S_{-0.1T}$ variation pattern of the GSDS1 profile. This similarity might be explained by the degree of contribution of possible maghemite with the high-temperature stability and relatively high coercivity of remanence. Note that in the GSDS2 profile IRMs were not measured because of the inapplicable shapes and sizes of the specimens to the related instruments. Second, we found a close similarity in variation of between ratios of MDF_{NRM} to MDF_{ARM} (MDF_{NRM}/MDF_{ARM}) from the two profiles. This can support within-site consistency in AF spectra of the acquired NRMs between the same depth levels. Figure 11 shows a possible stratigraphic correlation between the two profiles, which is made by matching major peak

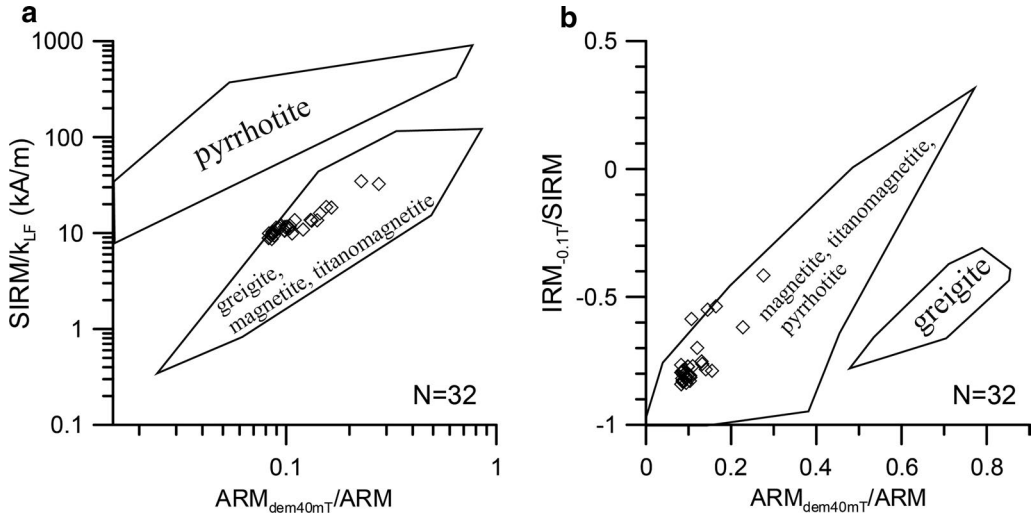

Fig. 8 **a** Biplot of SIRM/k_{LF} ratio versus $ARM_{dem40mT}$/ARM ratio, and **b** biplot of $IRM_{-0.1T}$/SIRM ratio versus $ARM_{dem40mT}$/ARM ratio, which are suggested by Peters and Thompson (1998) to discriminate "low-coercivity" magnetic minerals from each other, on the GSDS1 subsamples. Individual polygonal boxes denote the domains for identification of corresponding minerals from Peters and Thompson (1998)

values both in between the $S_{-0.1T}$ ratio and the $NRM_{580°C}$/$NRM_{20°C}$ ratio, and between the two MDF_{NRM}/MDF_{ARM} ratios, with variations of both NRM_{0mT}/ARM_{0mT} and NRM_{40mT}/ARM_{40mT} ratios at depth (possible proxies of paleointensity variation) as auxiliary data. This depth correlation makes downward shifts by 1.1–5.0 cm for the GSDS2 depth profile, confirming no significant difference in the upper and middle parts between the two profiles but more or less difference between the lower parts probably arisen from the sampling in the field. A line of estimated corrected depth (cmcd) data of the GSDS2 profile for the GSDS1 depth profile are given in Additional file 1: Table S4.

Figure 12 shows AF-derived NRM declinations and inclinations of the GSDS1 profile, and TH-derived NRM declinations and inclinations of the GSDS2 profile on the cmcd scale. In the figure, AF-derived LFC1 and HFC directions in the GSDS1 profile are illustrated as blue and red stars, respectively, and TH-derived LTC1, HTC1 and HTC2 directions in the GSDS2 profile are displayed as blue, red and yellow diamonds, respectively. Accordingly, note that the 8.2-to-55-cmcd (equivalent to the depth scale of the GSDS1 profile) interval has paleomagnetic data derived both from AF and TH demagnetization techniques. However, a first-order character is that there does not appear to be a similar pattern of variation between the high-demagnetization-level AF-derived (HFC) and TH-derived (HTC1 and, if present, HTC2) directions. For the 15-cmcd level (see Fig. 12), the HFC direction is identical to the LTC1 one, thus suggesting failure of the isolation of a higher-level remanence component in AF demagnetization. For the 55-cmcd level the LFC1 or HFC direction is analogous to that of the vector sum of the LTC1 and HTC1, indicating strong overlapping AF spectra of two possibly existing remanence components. Hence, we believe that some discrepancies of the high-level demagnetization-derived directions at the same levels are likely due to the incomplete separation of remanences by AF demagnetization resulting from the two remanence carriers (different Tc phases) with little difference in coercivity spectra, rather than suspicion of less within-site consistency of the directions.

The unusual NRM directions: rock magnetic anomalies or geomagnetic excursional behavior?

As described above, unusual NRM directions are seen in the high-demagnetization-level components (i.e. HTC1s or HFCs). We believe that the unusual directions were not influenced by the NRM of the underlying plateau-forming basalts (Kwanghaeak Basalts). Unfortunately, there is no NRM data of the nearby basalts so far, but the low-latitude plateau-forming basalts (which also belong to the Kwanghaeak Basalts) exposed along a southeast coast of Jeju Island, ~ 16 km away from the GSDS site, are broadly of normal polarity with $D = \sim 330°–355°$ and $I = \sim 50°–60°$ in the direction of characteristic remanence (ChRM) (Ahn, unpublished data). So, a key question is which one is the primary remanence (i.e. the geomagnetic field during or just after deposition) between LTC1 and HTC1.

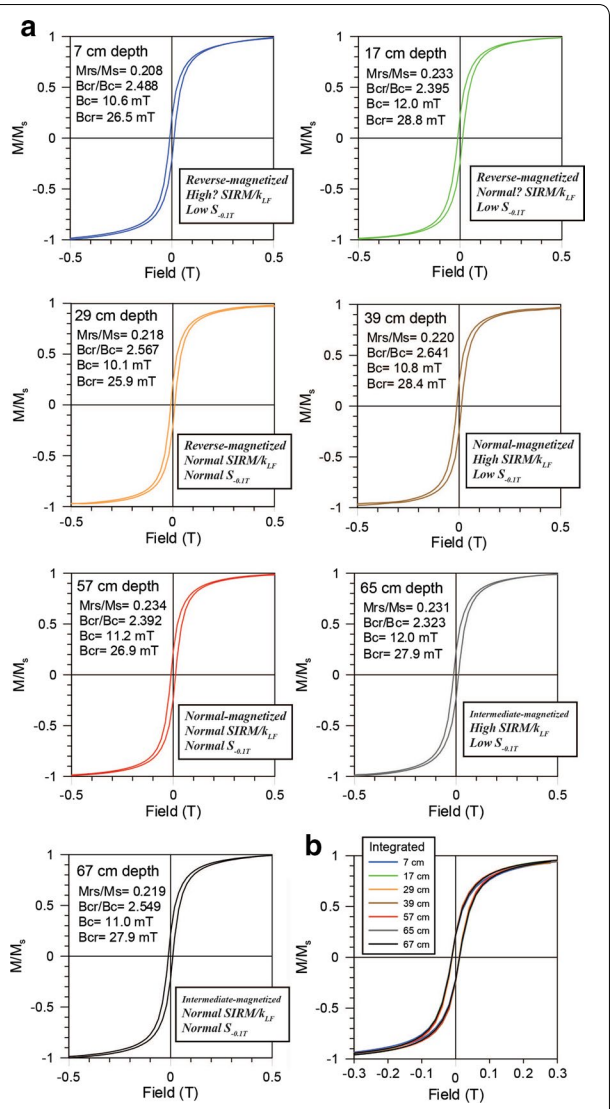

Fig. 9 **a** Magnetic hysteresis loops after correcting for the paramagnetic contribution at randomly selected different horizons (from 7 to 67 cm depth) of the GSDS1 profile, and **b** their integrated plots showing little or no differences between the loops

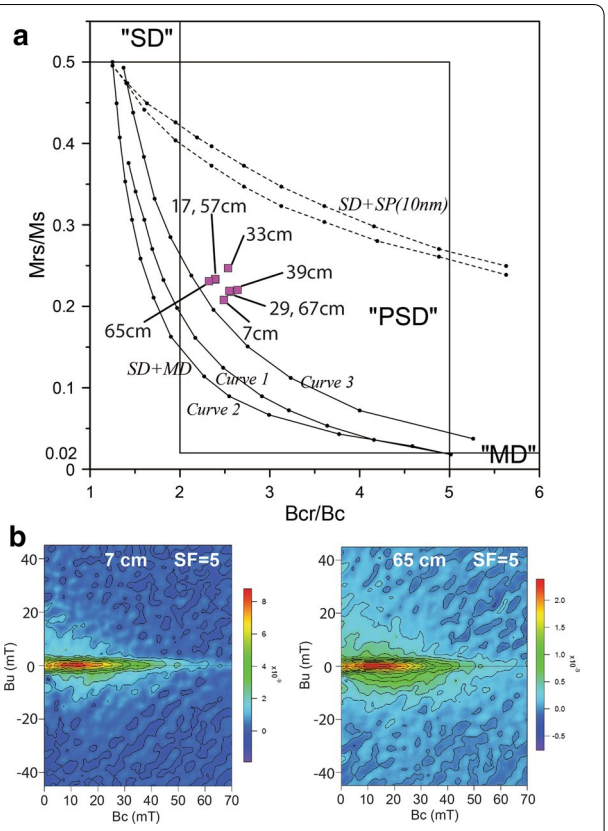

Fig. 10 **a** Day plot (Day et al. 1977) of hysteresis parameters on selected subsamples at different horizons (from 7 to 67 cm depth of the GSDS1 profile). Solid lines with dots denote theoretical curves 1–3 for mixtures of SD and MD grains, and dashed lines with dots indicate theoretical curves for mixtures of SD and SP (10 nm in size) grains (Dunlop 2002a, b). **b** Typical FORC diagrams for 7 and 65 cm subsamples

One could say that the LTC1 directions carried by possibly (occasionally maghemitized) Ti–rich titanomagnetite with Tc ~ 300 °C are primary. If so, the LTC1s should be DRMs. Also, even if partially low-temperature oxidation (maghemitization) of the detrital titanomagnetite grains occurs, the timing of the oxidation should be just after deposition, in which CRM can partially contribute to the NRM acquisition but its direction has to have little difference from the original DRM one. In this case, the magnetite (or Ti-poor titanomagnetite) grains must be chemical origin after deposition, because if the magnetite (or Ti-poor titanomagnetite) grains were also detrital in the origin, the HTC1 carried by the magnetite (or Ti-poor titanomagnetite) would have a similar direction as the LTC1 one.

Tarduno et al. (1996, 1998) suggested that, in pelagic sediments, chemical remanences carried by bacterial magnetite that is produced between the Mn- and Fe-redox boundaries can be acquired significantly after deposition with non-steady-state conditions. The CRM acquisition by bacterial magnetite could be a reason why the HTC1 directions are variable highly. However, there is no rock magnetic signature indicating the presence of bacterial magnetite [for example, dominance of SD magnetite expressed as e.g. $k_{ARM}/SIRM > \sim 1 \times 10^{-3}$ m/A and $k_{ARM}/k_{LF} > \sim 10$ and a sharp central ridge in the FORC diagram (e.g. Liu et al. 2015)].

Another possibility is that the HTC1 directions, carried possibly by magnetite (or Ti-poor titanomagnetite), are primary. If so, the HTC1s should be the original DRMs. Then the LTC1s should be post-depositional CRMs after

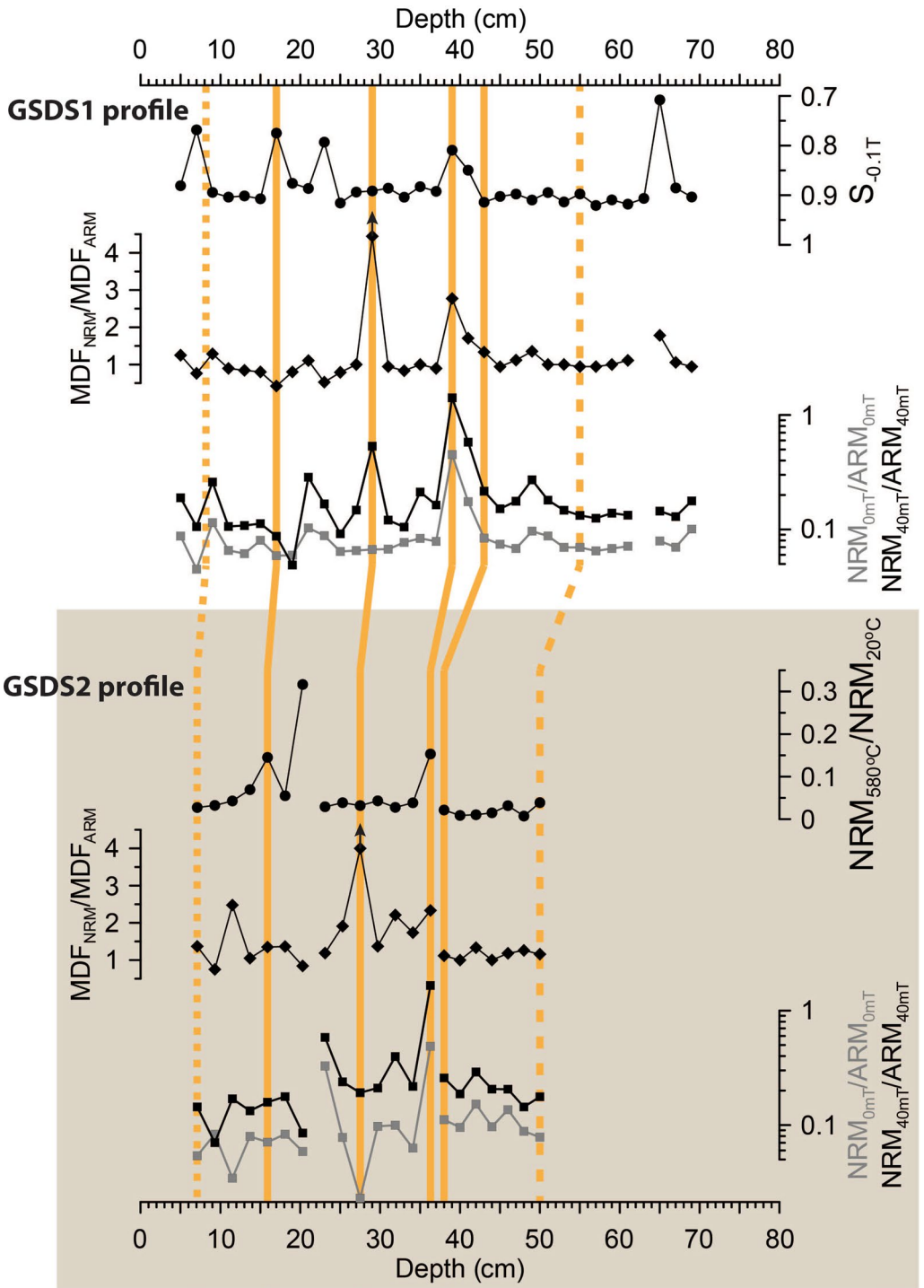

Fig. 11 A possible correlation of stratigraphic levels between GSDS1 and GSDS2 profiles, using rock magnetic parameters such as $S_{-0.1T}$ ratio, $NRM_{580°C}/NRM_{20°C}$ ratio, and MDF_{NRM}/MDF_{ARM} ratio, with the variations of NRM_{0mT}/ARM_{0mT} and NRM_{40mT}/ARM_{40mT} ratios (possible RPI proxies). Upward-pointing arrows in the MDF_{NRM}/MDF_{ARM}—depth graph denotes "higher than the value of the data point". This correlation enables the raw depth of the GSDS2 profile to convert into the GSDS1 depth scale (cmcd), with downward shifts by 1.1 cm for the 7.1–20.3 cm raw depth, by (0.9 + 0.3*x*) cm (*x*, distance between the raw depth and 23.1 cm) for the 23.1–36.3 cm raw depth, and by 5.0 cm for the 38.0–50.0 cm raw depth. See text for details

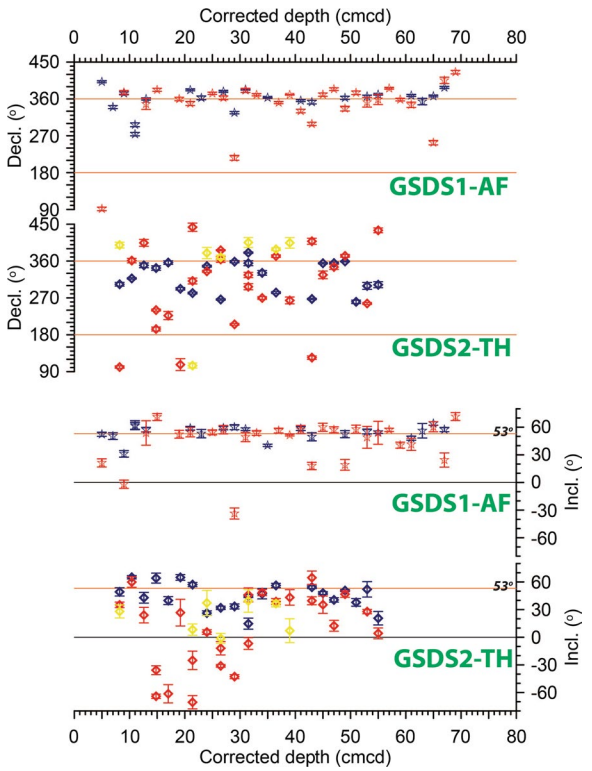

Fig. 12 AF-derived declinations and inclinations of the PCA-determined remanence components in the GSDS1 profile and TH-derived declinations and inclinations of the determined components in the GSDS2 profile, as a function of the corrected depth (cmcd, equivalent to the depth of the GSDS1 profile; see also Additional file 1: Table S3) by the rock magnetic GSDS1-GSDS2 correlation as in Fig. 11. Blue, red and yellow symbols denote the direction data of the components, LFC1 or LTC1, HFC or HTC1, and HTC2, respectively (see text for details). Error bar for the individual data points indicates the calculated MAD when applying the PCA. Note that direction data with MAD higher than 15° were not shown

deposition, compatible with the observation that the highest TH step that define the LTC1s is associated with the Tub (Tc) of the low-temperature mineral phase. This scenario is possible when the low-temperature oxidation of the original detrital (titano)magnetite to (titano)maghemite occurs (e.g. Bina and Prévot 1989; Zhou et al. 2001; Fischer et al. 2008; Channell and Xuan 2009) in oxidizing condition. It is also consistent with the LTC1 directions that are apparently within the secular variation range of the normal-polarity Brunhes Chron. Furthermore, this possibility may explain the occasional presence of the HTC2 having Tubs above 580 °C: some maghemite with high-temperature stability formed during the low-temperature oxidation might also acquire post-depositional CRM with Tubs with above 580 °C, having a normal-polarity direction, but this acquisition might not significantly affect the temperature spectra below 580 °C of its NRM previously carried by the detrital magnetite (or Ti-poor titanomagnetite), presumably because of a relatively little amount compared to the pre-existing magnetite (or Ti-poor titanomagnetite). This possible scenario may also explain the HTC1 decaying not toward the origin during TH demagnetization, for example, as shown in the case of specimen GSDS2–7.1 cm-TH of Fig. 4. On the other hand, some studies (e.g. Channell and Xuan 2009; Xuan and Channell 2010; Xuan et al. 2012) reported apparently negative inclinations unblocked below ~ 300–350 °C in late Brunhes-aged Arctic deep-sea sediments, which were often anti-parallel in direction to the remanence with higher Tubs. The low-temperature negative inclinations were interpreted by the authors as partially self-reversed CRMs carried by titanomaghemite. Even considering this, the current possibility that the HTC1 s were originated from the geomagnetic field during or just after deposition is still valid.

It would be also noted that in five depth levels (14.8, 21.4, 26.5, 31.5, 43.0 cmcd; 13.7, 20.3, 25.3, 29.7, 38.0 cm in the raw depth scale of the GSDS2 profile) the TH demagnetizations could isolate two different directions in the 280–580 °C range (Fig. 5; Fig. 12; Additional file 1: Table S4). It is difficult to find an exact explanation of the mechanism of these two remanence directions, but it is worth noting that at least for these distinct intervals there are some directional similarities to artifacts created by rock magnetic complexity discussed earlier. For solving this issue, more detailed identification of magnetic grains, for example, electron microscopy and X-ray analyses of magnetic separates may be helpful.

Figure 13a illustrates directional change of the HTC1s with time as the reversal angle (Valet et al. 2012) which denotes the angle between the local magnetic vector and the GAD-expected direction at the GSDS site ($D = 0°$, $I = 53°$). An estimated age-depth model based on linear interpolations between the AMS ^{14}C dates could assign a sequence of our paleomagnetic data to be in the age range from 21.3 to 17.1 cal. kyr BP (see also Additional file 1: Table S5), which is generally thought to be within the time of a stable normal magnetic field polarity (i.e. within the Brunhes Chron). The TH-derived paleomagnetic data possibly indicate variation of the geomagnetic field spanning approximately from 20.5 to 17.4 cal. kyr BP (or ka). This directional variation is characterized by several directional swings, where some reaches nearly the opposite polarity (~ 17.8 and ~ 18.6 ka), concentrated in the interval spanning approximately from 18.8 to 17.4 ka and by a possible high-amplitude departure at before ~ 20 ka. Figure 13b shows time-dependent variation in NRM_{40mT}/ARM_{40mT} ratio as a possible proxy of relative paleointensity (RPI) variation. This RPI proxy variation shows

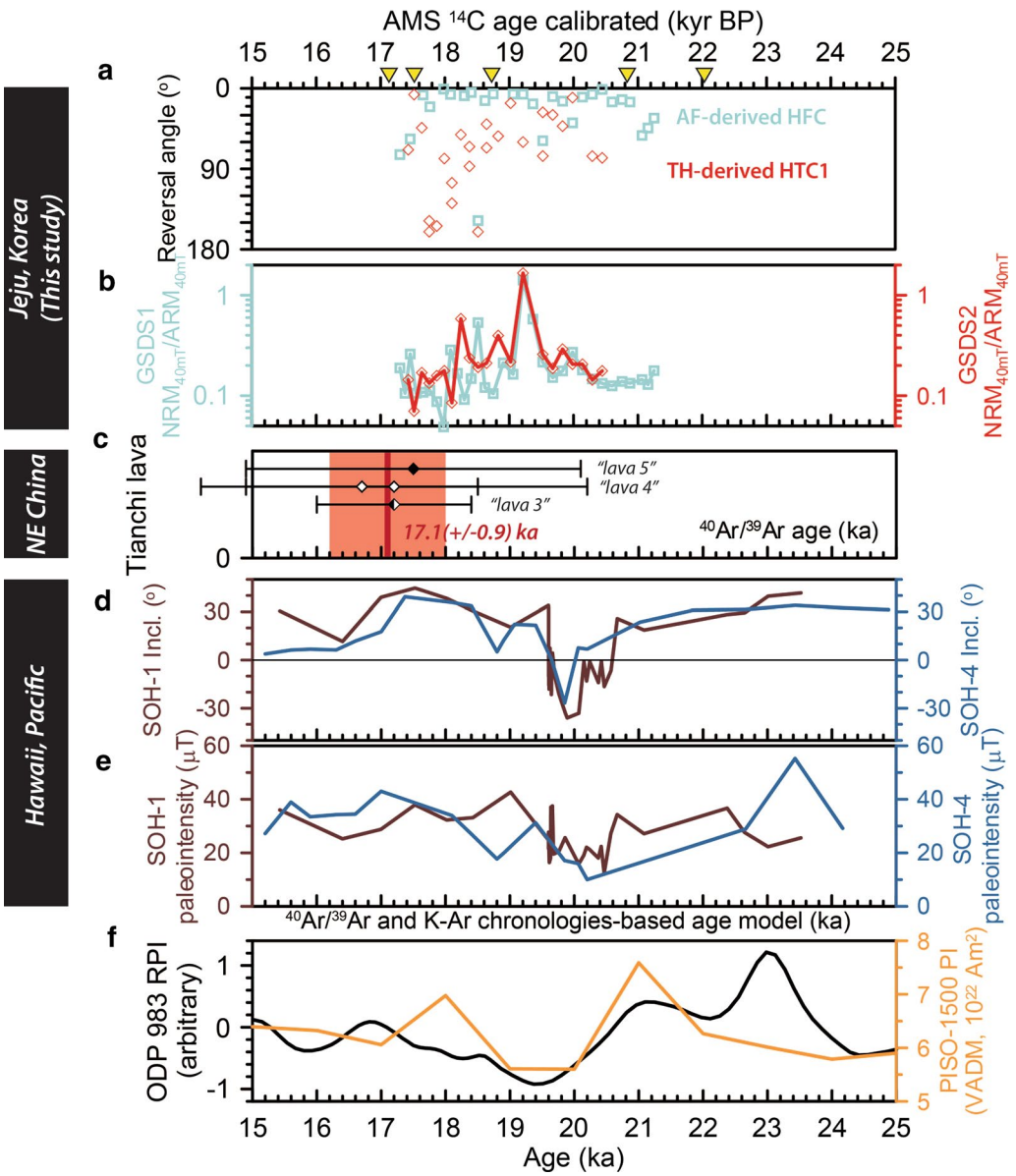

Fig. 13 Comparison of paleomagnetic data with anomalous directional features during 15–25 ka between the GSDS site (this study) and other different sites. **a** The GSDS1-AF-derived HFC and the GSDS2-TH-derived HTC1 directional changes, expressed as the reversal angle (the angle between the paleomagnetic direction and the direction of today's axial dipole field at the GSDS site) through time with our inferred age-depth model. Yellow reversed triangles indicate AMS ^{14}C dates directly determined by Lim et al. (2015). **b** NRM_{40mT}/ARM_{40mT} ratio (possible RPI proxy) variations through time with our inferred age-depth model in the GSDS site. **c** $^{40}Ar/^{39}Ar$ chronologies with the weighted mean of 17.1 ± 0.9 (2σ) ka (a red line and box) by Singer et al. (2014b) from the Tianchi comenditic lava sequence where both excursional directions and low absolute paleointensities were reported by Zhu et al. (2000). The individual age data, with 2σ uncertainties (error bars), are shown as open, half-filled, and filled diamond symbols indicating reversed, transitional, and normal polarities, respectively. **d**, **e** Temporal variations of paleomagnetic inclination and paleointensity retrieved from SOH-1 (brown lines; Teanby et al. 2002) and SOH-4 cores (blue lines; Laj et al. 2002b) in Hawaii, with their proposed $^{40}Ar/^{39}Ar$ and K–Ar chronologies-based age models. **f** Available time-dependent RPI records, with a $\delta^{18}O$ correlation-based age model, from ODP site 983 (Gardar Drift, North Atlantic) (Channell et al. 1997) and the PISO-1500 global RPI stack (Channell et al. 2009), as reference RPI curves

that there is extremely high at ~ 19.2 ka and relatively low values appear to persist over the periods before and after ~ 19.2 ka. A number of steady paleomagnetic studies with high-resolution and quasi-continuous deep-sea sediments have revealed that most excursions are associated with field intensity minima (e.g. Guyodo and Valet 1999; Stoner et al. 2002; Stott et al. 2002; Valet et al. 2005; Yamazaki and Oda 2005; Laj and Channell

2007; Channell et al. 2009; Roberts et al. 2013). However, we should note that in the studied sediment such RPI proxies based on AF-derived properties do not seem to ensure their validity probably because NRMs in the studied sediment are considered to be influenced entirely by the post-depositional CRMs having strongly overlapping AF spectra with those of the possible original DRMs, as discussed above.

In Table 1, previous paleomagnetic records of anomalous features during the 15–30 ka period are summarized. None of our unusual directional features, according to the estimated age model, could be correlated with the Rockall excursion (~ 26 ka; Channell et al. 2016). In the ~ 17–22 ka period that our paleomagnetic record covers, there are some documents reporting excursional features from different sites on the globe. Singer et al. (2014b) presented new $^{40}Ar/^{39}Ar$ dates of 17.1 ± 0.9 (2σ uncertainty; Fig. 13c) ka from comenditic lavas atop Tianchi Volcano in NE China, in which Zhu et al. (2000) reported excursional directions (corresponding to the intermediate-to-southerly VGP latitudes, labeled as "lava 3"and "lava 4" in Fig. 13c) and paleointensity lows, then they called it "Tianchi excursion". The authors suggested that the ~ 17 ka Tianchi excursion could be correlative with the Hilina Pali excursion that was first documented in Hawaii by Coe et al. (1978) and later confirmed by Laj et al. (2002b) and Teanby et al. (2002) (see also Fig. 13d, e), and even with some excursional records approximately between 17 and 20 ka from other sites (e.g. Peck et al. 1996; Nowaczyk and Knies 2000; Nowaczyk et al. 2003; Turrin et al. 2013). However, because of uncertainties on their chronologies the correlation still remains uncertain, as also pointed out in Singer et al. (2014b). On the other hand, it should be noted that in deep-sea sediment cores in eastern Arctic Ocean an apparent excursional feature (negative/shallow NRM inclinations) across the ~ 17–22 ka period was also observed (e.g. Nowaczyk and Knies 2000; Nowaczyk et al. 2003; Channell and Xuan 2009; Xuan and Channell 2010; Xuan et al. 2012), but some studies suggest that the Arctic excursional features are rock magnetic artifacts (e.g. Channell and Xuan 2009; Xuan and Channell 2010; Xuan et al. 2012). Moreover, in the given time interval, no excursional paleomagnetic directions but apparently high-amplitude secular variations in the direction were found in sedimentary cores from e.g. Laguna Potrok Aike maar lake in southern Argentina (Lisé-Pronovost et al. 2013) and western North Atlantic Ocean (Figures S1 to S3 in Lund et al. 2017).

To summarize, our recording of the unusual directions in the ~ 17–19 ka period may be correlative with the Tianchi excursion or elsewhere and, in conjunction with the possible large directional departure before ~ 20 ka, our paleomagnetic data may infer a possibility of more complex picture of the ~ 17–22 ka geomagnetic field than expected.

On the other hand, it is also fact that the previous quasi-continuous paleomagnetic records from lake or marine sediments in Northeast China (e.g. Frank 2007) and Japan (e.g. Yamazaki et al. 2003; Hayashida et al. 2007) did not preserve any excursional features (Additional file 1: Figure S1) despite relatively high sediment rates (~ 15 cm/kyr in Yamazaki et al. 2003; ~ 27 cm/kyr in Frank 2007; ~ 35 cm/kyr in Hayashida et al. 2007). However, the Tianchi lava sequence, although it is near Erlongwan maar lake, recorded the ~ 17 ka excursion (Singer et al. 2014b). One might say that the GSDS excursional features may be potentially correlated with any of inclination lows in the previous East Asia records (see Additional file 1: Figure S1), given that post-depositional remanence lock-in can smoothen geomagnetic signals with durations on time scales of hundreds of years (e.g. Channell and Guyodo 2004; Roberts and Winklhofer 2004).

Finally, we would like to emphasize the unusual directions we have observed need further investigation to confidently determine whether they record true geomagnetic instability or rock magnetic recording complexity.

Conclusion

Paleomagnetic and rock magnetic investigations were performed on a 64-cm-thick section of nonmarine unconsolidated muddy sediment (Gosan Formation) in Jeju Island, Korea, having an age interval of deposition between ~ 22 and ~ 17 ka. Interestingly, unusual NRM directions were found at several depths by stepwise AF demagnetizations, manifested by significantly large departures from the direction of today's axial dipole field. On the other hand, stepwise TH demagnetizations show more complex behavior resulting in the identification of multiple directional components, where two distinct components with TH steps between 120 and 240–320 °C (LTC1), and between 240–320 and 520–580 °C (HTC1), respectively, are predominant in all specimens analyzed. The low-temperature components (LTC1 s) generally indicate normal-polarity directions presumably within the secular variation range in the normal Brunhes Chron, whereas the high-temperature components (HTC1 s) often have unusual directions including negative inclinations and reversed directions, particularly in the ~ 13–34 cmcd (~ 17.6–18.8 ka in inferred age) and possibly below ~ 53 cmcd (before ~ 20.2 ka). A comprehensive interpretation from various rock magnetic analyses infers the co-existence of low-coercivity magnetic minerals having ~ 300 and ~ 580 °C Tcs, suggestive of (titano)maghemite and/or Ti–rich titanomagnetite

(not ferrimagnetic iron sulfides) and magnetite (or Ti-poor titanomagnetite). Some differences in directional behavior between AF and TH demagnetizations could be interpreted to result from incomplete separation, by the AF demagnetization, of the two remanence components with strongly overlapping AF spectra each other. Hence, it is possible that the low-temperature components may be associated with CRMs carried by (titano)maghemite probably formed by post-depositional low-temperature oxidation, and the high-temperature components might be primary geomagnetic records that survived from the post-depositional chemical influence. This therefore raises a possibility of geomagnetic instability within the ~ 17–22 ka period, manifested by multiple excursional swings, part of which might be associated with the Tianchi/Hilina Pali excursion. We note, however, that our interpretation of the excursional features is tentative and needs further works including electron microscopy and X-ray analyses of magnetic separates, and more thorough within-site consistency and between-site consistency checks for these excursional features to be considered true records of the geodynamo.

Additional file

Additional file 1. This includes a figure comparing paleomagnetic inclination data for East Asia from some previous literatures and this study (**Figure S1**), available AMS ^{14}C age data of the Gosan Formation (**Table S1**), some rock magnetic properties data (**Table S2**), AF-derived paleomagnetic direction data (**Table S3**), TH-derived paleomagnetic direction data (**Table S4**), and the estimated age-depth model data (**Table S5**) for the GSDS site of the Gosan Formation.

Abbreviations

^{14}C: radiocarbon; AF: alternating field; AGM: alternating gradient magnetometer; AMS: accelerator mass spectrometry; ARM: anhysteretic remanent magnetization; Bc: coercive force; Bcr: coercivity of remanence; ChRM: characteristic remanent magnetization; CMCR: the Center for Advanced Marine Core Research; CRM: chemical remanent magnetization; DANG: the angle between the PCA-determined directions with and without anchoring the origin; DC: direct current; DRM: detrital remanent magnetization; FORC: first-order reversal curve; GAD: geocentric axial dipole; GI: GRM index; GRM: gyroremanent magnetization; GSDS: a Gosan Formation exposure near Dangsanbong; GSF: Gosan Formation; GSSW: a Gosan Formation exposure near Suwolbong; HFC: remanence component with high AF demgnetization levels; HTC: high-temperature remanence component; IRM: isothermal remanent magnetization; k (k_{LF} and k_{HF}): magnetic susceptibility (with low- and high-frequency, respectively); KIGAM: the Korea Institute of Geoscience and Mineral Resources; LFC: remanence component with low AF demagnetization levels; LTC: low-temperature remanence component; MAD: maximum angular deviation; MD: multi-domain; MDF: median destructive field; Mrs: saturation remanent magnetization; Ms: saturation magnetization; NRM: natural remanent magnetization; OSL: optical stimulated luminescence; PCA: principal component analysis; PSD: pseudo-single domain; RPI: relative paleointensity; SAFD: stepwise alternating field demagnetization; SD: single domain; SIRM: saturated IRM; SP: superparamagnetic; STHD: stepwise thermal demagnetization; Tc: Curie temperature; TH: thermal; TOC: total organic carbon; TRM: thermoremanent magnetization; Tub: unblocking temperature; VGP: virtual geomagnetic pole.

Authors' contributions

JCK and H-SA collected the samples. H-SA carried out the paleomagnetic and rock magnetic measurements. All authors contributed to the discussion, and H-SA wrote the manuscript with the help from the other co-authors. All authors read and approved the final manuscript.

Author details

[1] Department of Geology and Research Institute of Natural Science, Gyeongsang National University, Jinju 52828, Republic of Korea. [2] Geologic Environment Division, Geo-Environmental Hazards and Quaternary Geology Research Center, Korea Institute of Geoscience and Mineral Resources (KIGAM), Daejeon 34132, Republic of Korea.

Acknowledgements

We are grateful to Professor Yuhji Yamamoto (CMCR of Kochi University, Japan), Dr. Youn Soo Lee (KIGAM, Korea), Dr. Hyeongseong Cho and Professor Moon Son (Pusan National University, Korea) for freely offering their laboratory facilities. Professor Y. Yamamoto is gratefully acknowledged for his critical comments to the initial manuscript of this paper. Dr. Norbert Nowaczyk, Dr. Chuang Xuan and Dr. Nicholas Teanby are kindly acknowledged for offering their published data. We thank the two anonymous reviewers and the lead guest editor of this special publication, Dr. John Tarduno, for constructive comments and suggestions which have considerably improved the manuscript. We are also grateful to Dr. John Tarduno for handling this paper and correcting English grammar. This work was supported by the Basic Science Research Program, "Full vector paleomagnetic records of volcanic rocks from Jeju Island", to H.-S.A. through the National Research Foundation of Korea (NRF-K) funded by the Ministry of Education (grant number NRF-2016R1D1A1B03935437).

Competing interests

The authors declare that they have no competing interests.

Ethics approval and consent to participate

Not applicable.

Publisher's Note

Received: 2 January 2018 Accepted: 25 April 2018
Published online: 09 May 2018

References

Ahn US, Choi HS (2016) Very young Gotjawal lavas (aged < ca. 10 ka) on Jeju Island, Korea: the major causes of Gotjawal formation. J Geol Soc Korea 52(4):433–441 **(in Korean with English abstract)**

Banerjee SK, King J, Marvin J (1981) A rapid method for magnetic granulometry with applications to environmental studies. Geophys Res Lett 8(4):333–336

Bhimasankaram V (1964) Partial magnetic self-reversal of pyrrhotite. Nature 202(4931):478–480

Bina M, Daly L (1994) Mineralogical change and self-reversed magnetizations in pyrrhotite resulting from partial oxidation; geophysical implications. Phys Earth Planet Int 85(1–2):83–99

Bina M, Prévot M (1989) Thermomagnetic investigations of titanomagnetite in submarine basalts: evidence for differential maghemitization. Phys Earth Planet Int 54(1–2):169–179

Bloemendal J, King J, Hall F, Doh SJ (1992) Rock magnetism of Late Neogene and Pleistocene deep-sea sediments: relationship to sediment source, diagenetic processes, and sediment lithology. J Geophys Res Solid Earth 97(B4):4361–4375

Brenna M, Németh K, Cronin SJ, Sohn YK, Smith IE, Wijbrans J (2015) Co-located monogenetic eruptions ~ 200 kyr apart driven by tapping vertically separated mantle source regions, Chagwido, Jeju Island, Republic of Korea. Bull Volcanol 77(5):43

Cassata WS, Singer BS, Cassidy J (2008) Laschamp and Mono Lake geomagnetic excursions recorded in New Zealand. Earth Planet Sci Lett 268(1):76–88
Cassidy J (2006) Geomagnetic excursion captured by multiple volcanoes in a monogenetic field. Geophys Res Lett 33:L21310
Channell J (2006) Late brunhes polarity excursions (mono lake, laschamp, iceland basin and pringle falls) recorded at odp site 919 (Irminger basin). Earth Planet Sci Lett 244(1):378–393
Channell JET, Guyodo Y (2004) The Matuyama Chronozone at ODP Site 982 (Rockall Bank): evidence for decimeter-scale magnetization lock-in depths. In: Channell JET et al. (eds) Timescales of the paleomagnetic Field. AGU Geophysical Monograph Seminar, vol 145. AGU, Washington, DC, pp 205–219
Channell J, Xuan C (2009) Self-reversal and apparent magnetic excursions in Arctic sediments. Earth Planet Sci Lett 284(1):124–131
Channell J, Hodell D, Lehman B (1997) Relative geomagnetic paleointensity and δ18 O at ODP Site 983 (Gardar Drift, North Atlantic) since 350 ka. Earth Planet Sci Lett 153(1):103–118
Channell J, Xuan C, Hodell D (2009) Stacking paleointensity and oxygen isotope data for the last 1.5 Myr (PISO-1500). Earth Planet Sci Lett 283(1):14–23
Channell J, Harrison R, Lascu I, McCave I, Hibbert F, Austin W (2016) Magnetic record of deglaciation using FORC-PCA, sortable-silt grain size, and magnetic excursion at 26 ka, from the Rockall Trough (NE Atlantic). Geochem Geophys Geosyst 17(5):1823–1841
Channell J, Riveiros NV, Gottschalk J, Waelbroeck C, Skinner L (2017) Age and duration of Laschamp and Iceland Basin geomagnetic excursions in the South Atlantic Ocean. Quat Sci Rev 167:1–13
Cheong C, Choi J, Sohn Y, Kim J, Jeong G (2007) Optical dating of hydromagmatic volcanoes on the southwestern coast of Jeju Island, Korea. Quat Geochronol 2(1):266–271
Clark H, Kennett J (1973) Paleomagnetic excursion recorded in latest Pleistocene deep-sea sediments, Gulf of Mexico. Earth Planet Sci Lett 19(2):267–274
Coe RS, Grommé S, Mankinen EA (1978) Geomagnetic paleointensities from radiocarbon-dated lava flows on Hawaii and the question of the Pacific nondipole low. J Geophys Res Solid Earth 83(B4):1740–1756
Day R, Fuller M, Schmidt VA (1977) Hysteresis properties of titanomagnetites: grain-size and compositional dependence. Phys Earth Planet Int 13:260–267
Doubrovine PV, Tarduno JA (2004) Self-reversed magnetization carried by titanomaghemite in oceanic basalts. Earth Planet Sci Lett 222(3):959–969
Doubrovine PV, Tarduno JA (2005) On the compositional field of self-reversing titanomaghemite: constraints from Deep Sea Drilling Project Site 307. J Geophys Res Solid Earth 110:B11104
Doubrovine PV, Tarduno JA (2006a) Alteration and self-reversal in oceanic basalts. J Geophys Res Solid Earth 111:B12S30
Doubrovine PV, Tarduno JA (2006b) N-type magnetism at cryogenic temperatures in oceanic basalt. Phys Earth Planet Int 157(1):46–54
Dunlop DJ (2002a) Theory and application of the Day plot (Mrs/Ms versus Hcr/Hc) 1. Theoretical curves and tests using titanomagnetite data. J Geophys Res Solid Earth 107:2056
Dunlop DJ (2002b) Theory and application of the Day plot (Mrs/Ms versus Hcr/Hc) 2. Application to data for rocks, sediments, and soils. J Geophys Res Solid Earth 107:2057
Evans M, Heller F (2003) Environmental magnetism: principles and applications of enviromagnetics. Academic Press, London
Fischer H, Luster J, Gehring A (2008) Magnetite weathering in a Vertisol with seasonal redox-dynamics. Geoderma 143(1–2):41–48
Fisher R (1953) Dispersion on a sphere. Proc R Soc Lond 217((Series A)):295–305
Frank U (2007) Palaeomagnetic investigations on lake sediments from NE China: a new record of geomagnetic secular variations for the last 37 ka. Geophys J Int 169(1):29–40
Fu Y, Von Dobeneck T, Franke C, Heslop D, Kasten S (2008) Rock magnetic identification and geochemical process models of greigite formation in Quaternary marine sediments from the Gulf of Mexico (IODP Hole U1319A). Earth Planet Sci Lett 275(3):233–245
Gehring AU, Fischer H, Louvel M, Kunze K, Weidler PG (2009) High temperature stability of natural maghemite: a magnetic and spectroscopic study. Geophys J Int 179(3):1361–1371
Gubbins D (1999) The distinction between geomagnetic excursions and reversals. Geophys J Int 137(1):F1–F3
Guyodo Y, Valet J-P (1999) Global changes in intensity of the Earth's magnetic field during the past 800 kyr. Nature 399(6733):249–252
Harrison RJ, Feinberg JM (2008) FORCinel: an improved algorithm for calculating first-order reversal curve distributions using locally weighted regression smoothing. Geochem Geophys Geosyst 9:Q05016
Hayashida A, Ali M, Kuniko Y, Kitagawa H, Torii M, Takemura K (2007) Environmental magnetic record and paleosecular variation data for the last 40 kyrs from the Lake Biwa sediments, Central Japan. Earth Planets Space 59(7):807–814. https://doi.org/10.1186/BF03352743
Hoffman KA, Singer BS (2008) Magnetic source separation in Earth's outer core. Science 321(5897):1800
Horng C-S, Torii M, Shea K-S, Kao S-J (1998) Inconsistent magnetic polarities between greigite-and pyrrhotite/magnetite-bearing marine sediments from the Tsailiao-chi section, southwestern Taiwan. Earth Planet Sci Lett 164(3):467–481
Itaki T, Ikehara K (2003) Radiolarian biozonation for the upper Quaternary in the Japan Sea. J Geol Soc Jpn 109(2):96–105
Jiang W-T, Horng C-S, Roberts AP, Peacor DR (2001) Contradictory magnetic polarities in sediments and variable timing of neoformation of authigenic greigite. Earth Planet Sci Lett 193(1):1–12
Kirschvink J (1980) The least-squares line and plane and the analysis of palaeomagnetic data. Geophys J Int 62(3):699–718
Koh GW, Park JB, Kang B-R, Kim G-P, Moon DC (2013) Volcanism in Jeju Island. J Geol Soc Korea 49(2):209–230 **(in Korean with English abstract)**
Krása D, Shcherbakov VP, Kunzmann T, Petersen N (2005) Self-reversal of remanent magnetization in basalts due to partially oxidized titanomagnetites. Geophys J Int 162(1):115–136
Laj C, Channell JET (2007) 5.10—Geomagnetic excursions A2. In: Schubert G (ed) Treatise on geophysics. Elsevier, Amsterdam, pp 373–416
Laj C, Kissel C, Mazaud A, Michel E, Muscheler R, Beer J (2002a) Geomagnetic field intensity, North Atlantic Deep Water circulation and atmospheric Δ 14 C during the last 50 kyr. Earth Planet Sci Lett 200(1):177–190
Laj C, Kissel C, Scao V, Beer J, Thomas DM, Guillou H, Muscheler R, Wagner G (2002b) Geomagnetic intensity and inclination variations at Hawaii for the past 98kyr from core SOH-4 (Big Island): a new study and a comparison with existing contemporary data. Phys Earth Planet Int 129(3):205–243
Laj C, Guillou H, Kissel C (2014) Dynamics of the earth magnetic field in the 10–75 kyr period comprising the Laschamp and Mono Lake excursions: new results from the French Chaîne des Puys in a global perspective. Earth Planet Sci Lett 387:184–197
Lee J, Kim J, Park J, Lim J, Hong S, Choi H (2014a) Age of volcanic activity from Quaternary deposits in Sangchang-ri, Jeju island. Korea. J Geol Soc Korea 50:697–706 **(in Korean with English abstract)**
Lee J-Y, Hong SS, Choi H, Nahm W-H, Lim J, Kim JC, Katsuki K (2014b) Preliminary geological interpretation of quaternary deposits between volcanic activities in Jeju island. In: Korea Institute of Geoscience and Mineral Resources (KIGAM), Daejeon, p 128 (**in Korean**)
Leonard GS, Calvert AT, Hopkins JL, Wilson CJN, Smid ER, Lindsay JM, Champion DE (2017) High-precision 40Ar/39Ar dating of Quaternary basalts from Auckland Volcanic Field, New Zealand, with implications for eruption rates and paleomagnetic correlations. J Volcanol Geotherm Res
Lim J, Lee J-Y, Kim JC, Hong SS, Choi H (2015) Paleoenvironmental and volcanologic implications of the Gosan Formation in Jeju Island, Korea. J Geol Soc Korea 51(6):537–544 **(in Korean with English abstract)**
Lisé-Pronovost A, St-Onge G, Gogorza C, Haberzettl T, Preda M, Kliem P, Francus P, Zolitschka B, Team TPS (2013) High-resolution paleomagnetic secular variations and relative paleointensity since the Late Pleistocene in southern South America. Quat Sci Rev 71:91–108
Liu S, Deng C, Xiao J, Li J, Paterson GA, Chang L, Yi L, Qin H, Pan Y, Zhu R (2015) Insolation driven biomagnetic response to the Holocene Warm Period in semi-arid East Asia. Sci Rep 5:8001
Lowrie W (1990) Identification of ferromagnetic minerals in a rock by coercivity and unblocking temperature properties. Geophys Res Lett 17(2):159–162

Lund S, Benson L, Negrini R, Liddicoat J, Mensing S (2017) A full-vector paleomagnetic secular variation record (PSV) from Pyramid Lake (Nevada) from 47–17 ka: evidence for the successive Mono Lake and Laschamp Excursions. Earth Planet Sci Lett 458:120–129
Macrì P, Sagnotti L, Dinarès-Turell J, Caburlotto A (2005) A composite record of Late Pleistocene relative geomagnetic paleointensity from the Wilkes Land Basin (Antarctica). Phys Earth Planet Int 151(3):223–242
Mochizuki N, Tsunakawa H, Shibuya H, Cassidy J, Smith IE (2006) Palaeointensities of the Auckland geomagnetic excursions by the LTD-DHT Shaw method. Phys Earth Planet Int 154(2):168–179
Noltimier H, Colinvaux P (1976) Geomagnetic excursion from Imuruk lake, Alaska. Nature 259(5540):197–200
Nowaczyk NR, Knies J (2000) Magnetostratigraphic results from the eastern Arctic Ocean: AMS 14C ages and relative palaeointensity data of the Mono Lake and Laschamp geomagnetic reversal excursions. Geophys J Int 140(1):185–197
Nowaczyk NR, Frederichs TW, Eisenhauer A, Gard G (1994) Magnetostratigraphic data from late quaternary sediments from the Yermak Plateau, Arctic Ocean: evidence For four geomagnetic polarity events within the last 170 Ka of the Brunhes Chron. Geophys J Int 117(2):453–471
Nowaczyk NR, Antonow M, Knies J, Spielhagen RF (2003) Further rock magnetic and chronostratigraphic results on reversal excursions during the last 50 ka as derived from northern high latitudes and discrepancies in precise AMS 14C dating. Geophys J Int 155(3):1065–1080
Nowaczyk N, Arz H, Frank U, Kind J, Plessen B (2012) Dynamics of the Laschamp geomagnetic excursion from Black Sea sediments. Earth Planet Sci Lett 351:54–69
O'reilly W (2012) Rock and mineral magnetism. Springer, Berlin
Özdemir Ö (1987) Inversion of titanomaghemites. Phys Earth Planet Int 46(1):184–196
Özdemir Ö, Banerjee SK (1984) High temperature stability of maghemite (γ-Fe2O3). Geophys Res Lett 11(3):161–164
Park KH, Lee B, Cho D, Kim J, Lee S, Choi H, Hwang J, Song G, Choi B, Cho B (1998) Geologic report of the Jeju-Aewol Sheet (1:50,000). Korea Institute Geology, Mining and Materials, Taejon 290 (**in Korean with English abstract**)
Park KH, Cho D, Kim J (2000a) Geologic report of the Mosulpo-Hanrim Sheet (1:50,000). Korea Institute Geology, Mining and Materials, Taejon, p 56 (**in Korean with English abstract**)
Park KH, Cho D, Kim Y, Kim J, Cho B, Jang Y, Lee B, Lee S, Son B, Cheon H (2000b) Geologic report of the Seogwipo-Hahyori Sheet (1:50,000). Jeju Provincial Government 163 (**in Korean with English abstract**)
Park J, Lim HS, Lim J, Yu KB, Choi J (2014) Orbital-and millennial-scale climate and vegetation changes between 32.5 and 6.9 kcal a BP from Hanon Maar paleolake on Jeju Island, South Korea. J Quat Sci 29(6):570–580
Peck J, King J, Colman SM, Kravchinsky V (1996) An 84-kyr paleomagnetic record from the sediments of Lake Baikal, Siberia. J Geophys Res Solid Earth 101(B5):11365–11385
Peters C, Thompson R (1998) Magnetic identification of selected natural iron oxides and sulphides. J Magn Magn Mater 183(3):365–374
Quane S, Garcia M, Guillou H, Hulsebosch T (2000) Magmatic history of the East Rift Zone of Kilauea Volcano, Hawaii based on drill core from SOH 1. J Volcanol Geoth Res 102(3):319–338
Rieck HJ, Sarna-Wojcicki AM, Meyer CE, Adam DP (1992) Magnetostratigraphy and tephrochronology of an upper Pliocene to Holocene record in lake sediments at Tulelake, Northern California. GSA Bull 104(4):409–428
Roberts AP, Weaver R (2005) Multiple mechanisms of remagnetization involving sedimentary greigite (Fe3S4). Earth Planet Sci Lett 231(3):263–277
Roberts AP, Winklhofer M (2004) Why are geomagnetic excursions not always recorded in sediments? Constraints from post-depositional remanent magnetization lock-in modelling. Earth Planet Sci Lett 227(3):345–359
Roberts AP, Pike CR, Verosub KL (2000) First-order reversal curve diagrams: a new tool for characterizing the magnetic properties of natural samples. J Geophys Res Solid Earth 105(B12):28461–28475
Roberts AP, Chang L, Rowan CJ, Horng CS, Florindo F (2011) Magnetic properties of sedimentary greigite (Fe3S4): an update. Rev Geophy 49:RG1002
Roberts AP, Tauxe L, Heslop D (2013) Magnetic paleointensity stratigraphy and high-resolution Quaternary geochronology: successes and future challenges. Quat Sci Rev 61:1–16
Rowan CJ, Roberts AP (2006) Magnetite dissolution, diachronous greigite formation, and secondary magnetizations from pyrite oxidation: unravelling complex magnetizations in Neogene marine sediments from New Zealand. Earth Planet Sci Lett 241(1):119–137
Rubin M, Berthold SM (1961) US geological survey radiocarbon dates VI*. Radiocarbon 3:86–98
Sagnotti L, Roberts AP, Weaver R, Verosub KL, Florindo F, Pike CR, Clayton T, Wilson GS (2005) Apparent magnetic polarity reversals due to remagnetization resulting from late diagenetic growth of greigite from siderite. Geophys J Int 160(1):89–100
Shibuya H, Cassidy J, Smith I, Itaya T (1992) A geomagnetic excursion in the Brunhes epoch recorded in New Zealand basalts. Earth Planet Sci Lett 111(1):41–48
Singer BS (2014) A Quaternary geomagnetic instability time scale. Quat Geochronol 21:29–52
Singer BS, Hoffman KA, Schnepp E, Guillou H (2008) Multiple Brunhes Chron excursions recorded in the West Eifel (Germany) volcanics: support for long-held mantle control over the non-axial dipole field. Phys Earth Planet Int 169(1):28–40
Singer BS, Jicha BR, Condon DJ, Macho AS, Hoffman KA, Dierkhising J, Brown MC, Feinberg JM, Kidane T (2014a) Precise ages of the Réunion event and Huckleberry Ridge excursion: episodic clustering of geomagnetic instabilities and the dynamics of flow within the outer core. Earth Planet Sci Lett 405:25–38
Singer BS, Jicha BR, He H, Zhu R (2014b) Geomagnetic field excursion recorded 17 ka at Tianchi Volcano, China: new 40Ar/39Ar age and significance. Geophys Res Lett 41(8):2794–2802
Sohn YK, Chough SK (1989) Depositional processes of the Suwolbong tuff ring, Cheju Island (Korea). Sedimentology 36(5):837–855
Sohn YK, Park KH (2004) Early-stage volcanism and sedimentation of Jeju Island revealed by the Sagye borehole, SW Jeju Island, Korea. Geosci J 8(1):73
Sohn YK, Park KH (2005) Composite tuff ring/cone complexes in Jeju Island, Korea: possible consequences of substrate collapse and vent migration. J Volcanol Geotherm Res 141(1):157–175
Sohn YK, Park KH, Yoon SH (2008) Primary versus secondary and subaerial versus submarine hydrovolcanic deposits in the subsurface of Jeju Island, Korea. Sedimentology 55(4):899–924
Stoner J, Laj C, Channell J, Kissel C (2002) South Atlantic and North Atlantic geomagnetic paleointensity stacks (0–80 ka): implications for interhemispheric correlation. Quat Sci Rev 21(10):1141–1151
Stott L, Poulsen C, Lund S, Thunell R (2002) Super ENSO and global climate oscillations at millennial time scales. Science 297(5579):222–226
Tarduno JA, Wilkison SL (1996) Non-steady state magnetic mineral reduction, chemical lock-in, and delayed remanence acquisition in pelagic sediments. Earth Planet Sci Lett 144(3–4):315–326
Tarduno JA, Tian W, Wilkison S (1998) Biogeochemical remanent magnetization in pelagic sediments of the western equatorial Pacific Ocean. Geophys Res Lett 25(21):3987–3990
Tarduno JA, Watkeys MK, Huffman TN, Cottrell RD, Blackman EG, Wendt A, Scribner CA, Wagner CL (2015) Antiquity of the South Atlantic Anomaly and evidence for top-down control on the geodynamo. Nat Commun 6:7865
Tauxe L (2010) Essentials of paleomagnetism. University of California Press, California
Teanby N, Laj C, Gubbins D, Pringle M (2002) A detailed palaeointensity and inclination record from drill core SOH1 on Hawaii. Phys Earth Planet Int 131(2):101–140
Thébault E, Finlay CC, Beggan CD, Alken P, Aubert J, Barrois O, Bertrand F, Bondar T, Boness A, Brocco L (2015) International geomagnetic reference field: the 12th generation. Earth Planets Space 67(1):1–19. https://doi.org/10.1186/s40623-015-0228-9
Turrin BD, Champion DE, Mortlock RA, Fairbanks RG, Swisher CC (2013) 40Ar/39Ar and U-series ages of a Late Pleistocene geomagnetic excursion in Western North America: The Halina Pali event in Western North America? AGU Fall Meeting Abstract Program:GP31A-06
Valet J-P, Meynadier L, Guyodo Y (2005) Geomagnetic dipole strength and reversal rate over the past two million years. Nature 435(7043):802
Valet JP, Fournier A, Courtillot V, Herrero-Bervera E (2012) Dynamical similarity of geomagnetic field reversals. Nature 490(7418):89–93
Weaver R, Roberts AP, Barker AJ (2002) A late diagenetic (syn-folding) magnetization carried by pyrrhotite: implications for paleomagnetic studies

from magnetic iron sulphide-bearing sediments. Earth Planet Sci Lett 200(3):371–386
Xuan C, Channell JE (2010) Origin of apparent magnetic excursions in deep-sea sediments from Mendeleev-Alpha Ridge, Arctic Ocean. Geochem Geophys Geosyst 11:Q02003
Xuan C, Channell JE, Polyak L, Darby DA (2012) Paleomagnetism of Quaternary sediments from Lomonosov Ridge and Yermak Plateau: implications for age models in the Arctic Ocean. Quat Sci Rev 32:48–63
Yamazaki T, Oda H (2005) A geomagnetic paleointensity stack between 0.8 and 3.0 Ma from equatorial Pacific sediment cores. Geochem Geophys Geosyst 6:Q11H20
Yamazaki T, Abdeldayem AL, Ikehara K (2003) Rock-magnetic changes with reduction diagenesis in Japan Sea sediments and preservation of geomagnetic secular variation in inclination during the last 30,000 years. Earth Planets Space 55(6):327–340. https://doi.org/10.1186/BF03351766
Yaskawa K, Nakajima T, Kawai N, Torii M, Natsuhara N, Horie S (1973) Palaeomagnetism of a core from Lake Biwa (I). J Geomagn Geoelectr 25(4):447–474
Zhang K, Gubbins D (2000) Is the geodynamo process intrinsically unstable? Geophys J Int 140(1):F1–F4
Zhou W, Van der Voo R, Peacor DR, Wang D, Zhang Y (2001) Low-temperature oxidation in MORB of titanomagnetite to titanomaghemite: a gradual process with implications for marine magnetic anomaly amplitudes. J Geophys Res Solid Earth 106(B4):6409–6421
Zhu R, Pan Y, Coe RS (2000) Paleointensity studies of a lava succession from Jilin Province, northeastern China: evidence for the Blake event. J Geophys Res Solid Earth 105(B4):8305–8317
Zijderveld JDA (1967) A. C. demagnetization of rocks: analysis of results. Elsevier, Amsterdam